

THE EFFECT OF LITHIUM ION ON THE DEGRADATION
OF DIPHOSPHATE ANION IN MOLTEN ALKALI NITRATES

by

ARTHUR STEVEN METCALF

B.A. Kansas State Teachers College, 1972

A MASTER'S THESIS

submitted in partial fulfillment of the

requirements for the degree


MASTER OF SCIENCE

Department of Chemistry

KANSAS STATE UNIVERSITY
Manhattan, Kansas

1975

Approved by:


Major Professor

LD
2668
T4
1975
M47
C 2
Document

TABLE OF CONTENTS

LIST OF FIGURES	ii
LIST OF TABLES	v
INTRODUCTION	1
I. Purpose of This Investigation	1
II. Background	2
A. Molten Nitrate Solvent	2
B. Condensed Phosphates	6
C. Solvolytic Scission of the Diphosphate Anion by Molten Lithium Nitrate	10
D. Hydrolysis of the Diphosphate Anion as a Function of pH	18
EXPERIMENTAL	21
I. Chemicals	21
II. Apparatus	21
A. Constructed Apparatus	21
B. Commercial Apparatus	23
III. Quenched Reaction Kinetic Studies	24
A. 70-30 mol % LiNO_3 - NaNO_3	24
B. 80-20 mol % LiNO_3 - NaNO_3	25
C. 90-10 mol % LiNO_3 - NaNO_3	26
RESULTS AND DISCUSSION	27
SUMMARY AND CONCLUSIONS	71
ACKNOWLEDGMENTS	73
LITERATURE CITED	74
VITA	76

LIST OF FIGURES

Fig. 1.	Structures of several typical condensed phosphate anions . . .	7
Fig. 2.	Plots of Hubble's data of the natural logarithm of the fraction of phosphorus remaining as $P_2O_7^{4-}$, $\ln X_{DP}$, <u>versus</u> time, t (min), at various temperatures for the reaction of $P_2O_7^{4-}$ with excess molten $LiNO_3$ where the cation mole percent of Li^+ is 93.23 mol %	16
Fig. 3.	Plots of the common logarithm of the first order rate constants, $\log k_1$, <u>versus</u> $1/T$ ($^{\circ}K$) $^{-1}$ for the hydrolysis of $P_2O_7^{4-}$ at various pH's	19
Fig. 4.	Plots of the common logarithm of the first order rate constants, $\log k_1$, <u>versus</u> pH for the hydrolysis of the diphosphate anion. Curve (a) is for γ -phenylpropyl diphosphate at 95° . Remaining curves are for inorganic diphosphate at (b) 90° ; (c) 69° ; (d) 65.50° ; (e) 60° ; and (f) 40° (6)	20
Fig. 5.	Quenched reaction vessel. A and B are the outer and inner jackets, respectively. D is the innermost glass tube, (called the plunger) G is a metal spring, F is a cork, E is the beveled flange, C is an entrance opening for charging the inner jacket with diphosphate reactant, and H represents the metal washers	22
Fig. 6.	Time average ^{31}P nmr spectrum of an aqueous sample obtained from the $Na_4P_2O_7$ - $LiNO_3$ reaction at 342° quenched after 15 min at a Li^+ concentration of 74.31 cation mol %	34
Fig. 7.	Plots of the natural logarithm of the fraction of unreacted diphosphate anion, $\ln X_{DP}$, <u>versus</u> reaction time, t (min), at 337 and 342° at a concentration of Li^+ of 65.30 cation mol %	37
Fig. 8.	Plots of the natural logarithm of the fraction of unreacted diphosphate anion, $\ln X_{DP}$, <u>versus</u> reaction time, t (min), at 347 and 352° at a concentration of Li^+ of 65.30 cation mol %	39
Fig. 9.	Plots of the natural logarithm of the fraction of unreacted diphosphate anion, $\ln X_{DP}$, <u>versus</u> reaction time, t (min), at 337 and 342° at a concentration of Li^+ of 74.31 cation mol %	41
Fig.10.	Plots of the natural logarithm of the fraction of unreacted diphosphate anion, $\ln X_{DP}$, <u>versus</u> reaction time, t (min), at 347 and 352° at a concentration of Li^+ of 74.31 cation mol %	43

- Fig. 11. Plots of the natural logarithm of the fraction of unreacted diphosphate anion, $\ln X_{DP}$, versus reaction time, t (min), at 337 and 342° at a concentration of Li^+ of 83.77 cation mol % 45
- Fig. 12. Plots of the natural logarithm of the fraction of unreacted diphosphate anion, $\ln X_{DP}$, versus reaction time, t (min), at 347 and 352° at a concentration of Li^+ of 83.77 cation mol % 47
- Fig. 13. Plots of the natural logarithm of the first order rate constants, $\ln k_1$, versus $1/T$ ($^{\circ}K$)⁻¹ for the $Na_4P_2O_7$ - $LiNO_3$ reaction at 65.30, 74.31, 83.77 and 93.23 cation mol % . . . 49
- Fig. 14. Plots of the natural logarithm of k_1/T (min $^{\circ}K$)⁻¹, $\ln k_1/T$, versus $1/T$ ($^{\circ}K$)⁻¹ for the $Na_4P_2O_7$ - $LiNO_3$ reaction at 65.30, 74.31, 83.77 and 93.23 cation mol % 52
- Fig. 15. Plots of the natural logarithm of the fraction of unreacted diphosphate anion, $\ln X_{DP}$, versus reaction time, t (min), at various temperatures for the reaction of $P_2O_7^{4-}$ in molten $LiNO_3$ solvent of 65.30 cation mol % Li^+ 55
- Fig. 16. Plots of the natural logarithm of the fraction of unreacted diphosphate anion, $\ln X_{DP}$, versus reaction time, t (min), at various temperatures for the reaction of $P_2O_7^{4-}$ in molten $LiNO_3$ solvent of 74.31 cation mol % Li^+ 57
- Fig. 17. Plots of the natural logarithm of the fraction of unreacted diphosphate anion, $\ln X_{DP}$, versus reaction time, t (min), at various temperatures for the reaction of $P_2O_7^{4-}$ in molten $LiNO_3$ solvent of 83.77 cation mol % Li^+ 59
- Fig. 18. Plots of the natural logarithm of the fraction of unreacted diphosphate anion, $\ln X_{DP}$, versus reaction time, t (min), at various Li^+ concentrations for the reaction of $P_2O_7^{4-}$ in molten $LiNO_3$ solvent at 337° 61
- Fig. 19. Plots of the natural logarithm of the fraction of unreacted diphosphate anion, $\ln X_{DP}$, versus reaction time, t (min), at various Li^+ concentrations for the reaction of $P_2O_7^{4-}$ in molten $LiNO_3$ solvent at 342° 63
- Fig. 20. Plots of the natural logarithm of the fraction of unreacted diphosphate anion, $\ln X_{DP}$, versus reaction time, t (min), at various Li^+ concentrations for the reaction of $P_2O_7^{4-}$ in molten $LiNO_3$ solvent at 347° 65
- Fig. 21. Plots of the natural logarithm of the fraction of unreacted diphosphate anion, $\ln X_{DP}$, versus reaction time, t (min), at various Li^+ concentrations for the reaction of $P_2O_7^{4-}$ in molten $LiNO_3$ solvent at 352° 67

Fig. 22. Plots of the common logarithm of the first order rate constants, $\log k_1 \text{ (min)}^{-1}$, versus the negative common logarithm of the Li^+ cation concentration, pLi , at various temperatures 69

LIST OF TABLES

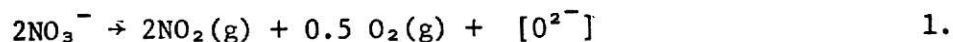
Table 1.	Rate and equilibrium data for the reactions of pyro-sulfate and dichromate ions with fused alkali nitrates . .	4
Table 2.	Summary of residual $P_2O_7^{4-}$ content at various times at 337, 342, 347 and 352°, first order rate constants, and activation energy and entropy for the $LiNO_3$ (x's) + $Na_4P_2O_7$ reaction	13
Table 3.	Summary of residual $P_2O_7^{4-}$ and PO_4^{3-} content at various times at 337 and 342° at a Li^+ concentration of 65.30 cation mol % and first order rate constants for the reaction $Na_4P_2O_7-LiNO_3$	28
Table 4.	Summary of residual $P_2O_7^{4-}$ and PO_4^{3-} content at various times at 347 and 352° at a Li^+ concentration of 65.30 cation mol % and first order rate constants for the reaction $Na_4P_2O_7-LiNO_3$	29
Table 5.	Summary of residual $P_2O_7^{4-}$ and PO_4^{3-} content at various times at 337 and 342° at a Li^+ concentration of 74.31 cation mol % and first order rate constants for the reaction $Na_4P_2O_7-LiNO_3$	30
Table 6.	Summary of residual $P_2O_7^{4-}$ and PO_4^{3-} content at various times at 347 and 352° at a Li^+ concentration of 74.31 cation mol % and first order rate constants for the reaction $Na_4P_2O_7-LiNO_3$	31
Table 7.	Summary of residual $P_2O_7^{4-}$ and PO_4^{3-} content at various times at 337 and 342° at a Li^+ concentration of 83.77 cation mol % and first order rate constants for the reaction $Na_4P_2O_7-LiNO_3$	32
Table 8.	Summary of residual $P_2O_7^{4-}$ and PO_4^{3-} content at various times at 337 and 352° at a Li^+ concentration of 83.77 cation mol % and first order rate constants for the reaction $Na_4P_2O_7-LiNO_3$	33
Table 9.	Summary of activation energies and entropies calculated from an Arrhenius plot and from a plot of $\ln (k_1/T)$ versus $(1/T) (^{\circ}K)^{-1}$ and least squares equations for best straight lines from both plots at various Li^+ concentrations	53

INTRODUCTION

I. Purpose of This Investigation

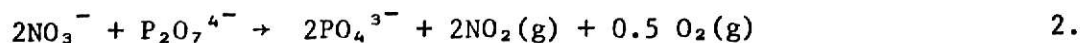
In the last 10-12 years several studies of molten nitrates as solvents have been conducted (1,2). The reactions in solvolysis by molten nitrates involve the net transfer of an oxide ion, O^{2-} . This type of reaction has been labeled an acid-base reaction by Lux (3), as further supported by Flood, *et al.* (4). The acid-base nature arises out of an extension of the Lewis acid-base theory. The Lux-Flood definition is that an acid is an oxide ion acceptor and a base is an oxide ion donor.

An earlier study made in our laboratory by L. Gutierrez (5) concerned use of the nitrate anion (as $NaNO_3$) as a Lux-Flood base with several condensed phosphates as acids. The net reaction for the nitrate is:



where $[O^{2-}]$ denotes an oxide ion donation and not a real concentration of oxide ion. The reactions were conducted at several temperatures to obtain stoichiometries and kinetics. The phosphate anions were depolymerized to the diphosphate anion, $P_2O_7^{4-}$, upon reaction with molten nitrate. This was the result of using sodium salts for the nitrate and the phosphates. However, when Gutierrez made a stoichiometric study of the reaction of lithium nitrate, $LiNO_3$, with sodium cyclic trimetaphosphate, $Na_3(PO_3)_3$, the final degradation product was PO_4^{3-} . This seemed to indicate a cation effect in going from the sodium to the lithium salt.

In the unpublished work of B. R. Hubble done in our laboratory in the summer of 1974, the reaction of $LiNO_3$ with $Na_4P_2O_7$ was kinetically studied. The reaction was:



The degradation of the $\text{P}_2\text{O}_7^{4-}$ anion to PO_4^{3-} was observed to be first order with respect to $\text{P}_2\text{O}_7^{4-}$. The reaction was carried out in a 55:1 mole ratio of LiNO_3 to $\text{Na}_4\text{P}_2\text{O}_7$. The diphosphate-lithium nitrate reaction was kinetically studied in the present work at various temperatures and lithium cation concentrations. The lithium concentration was controlled by dilution of molten lithium nitrate with sodium nitrate, the latter which had been found by Gutierrez to give no reaction with the diphosphate anion. The present studies are similar to those conducted on the hydrolysis of the diphosphate anion as a function of pH (6). Thus, comparison will be made, where possible, between the scission of $\text{P}_2\text{O}_7^{4-}$ as a function of lithium ion concentration, and the hydrolysis as a function of pH.

In this work the following are included: (a) kinetics of the $\text{Na}_4\text{P}_2\text{O}_7$ - LiNO_3 reaction from 337 to 352 $^\circ$, followed by observing integrated intensity changes in the ^{31}P nmr spectra of quenched reaction samples dissolved in de-ionized water; (b) kinetics of the above reaction from 70 to 90 mol % lithium nitrate, also followed by observing integrated intensity changes in the ^{31}P nmr spectra of quenched reaction samples; (c) comparisons of kinetic data as functions of temperature and Li^+ concentration; (d) comparison of rate constants as functions of Li^+ concentration at the various temperatures; (e) calculation of activation energy and entropy at each Li^+ concentration; and (f) interpretation of the results and discussion with respect to proposed mechanisms.

II. Background

A. Molten Nitrate Solvent

Fused salt solvents with polyatomic oxyanions, such as nitrates, are characterized as acid-base systems by the Lux-Flood theory (3,4). As stated previously this theory deals with the effective donation of an oxide ion, O^{2-} . The nitrate anion as a base undergoes the net reaction 1 in these acid-base systems. In this reaction $[\text{O}^{2-}]$ denotes the transfer of the oxide ion (7).

The effect on the Lux-Flood acid is varied upon reaction with an oxide ion donating base (5). This variance is to a large degree dependent on the ionization energy of the central atoms which compose the acid species. Acids composed of central atoms with high ionization energies exhibit a change in

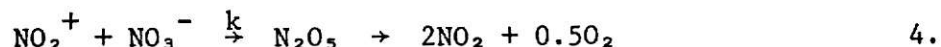
the central atom's coordination number for oxygen upon reaction with a base. Acids composed of central atoms with low ionization energies exhibit the formation of an oxide phase upon reaction with a base. The medium ionization energy atoms give the most interesting results upon reaction. Acids containing central atoms of this nature are largely polymeric in structure with oxygen bridging. Reactions of these acids yield a rupturing of these bridges with simultaneous addition of an oxide ion to form smaller structures.

The acid-base equilibrium involved in molten nitrates has been a very controversial topic over the last few years. Controversies have arisen over the nature of the acidic and basic species. The acidic species has been proposed by Duke and Kust (8) as NO_2^+ , while Topol, *et al.*, (9) has attempted to prove the species to be NO_2 . The center of the argument concerning the basic species is the principal form of oxygen ion present in the molten nitrates. The oxide ion, O^{2-} , is favored by Duke and Kust (8) and Topol, *et al.*, (9), while Zambonin and Jordan (10) have supported the superoxide ion, O_2^- .

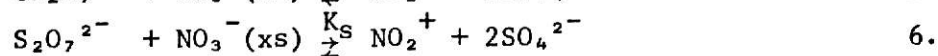
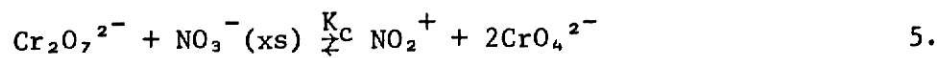
Duke and Kust (8) postulated the equilibrium for a pure sodium-potassium nitrate eutectic as:



followed by



In an attempt to verify the proposed acid species, NO_2^+ , Duke reported values for the equilibrium constant, K_1 , of $(2.7 \pm 0.3) \times 10^{-26}$ and $(5.7 \pm 0.1) \times 10^{-24}$ at 250 and 300°, respectively. These values were determined potentiometrically. In a previous study by Duke and Yamamoto (11) the following equilibria were examined:



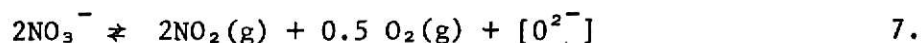
along with the rate of reaction 4. The values of the equilibrium constants (K_c and K_s) and the rate constant (k) were obtained for the above reactions

in molten nitrate. Table 1 contains the results of this study, including the above constants, with the enthalpies for the equilibrium reactions (ΔH) and enthalpy of activation (ΔH_a) for reaction 4 (11).

Table 1. Rate and equilibrium data for the reactions of pyrosulfate and dichromate ions with fused alkali nitrates.

$\frac{k}{(\text{min}^{-1})}$	$T(^{\circ}\text{C})$	$K_S(\text{S}_2\text{O}_7^{2-})$	$T(^{\circ}\text{C})$	$K_C(\text{Cr}_2\text{O}_7^{2-})$
0.038	235	0.026	250	8.5×10^{-14}
0.096	275	0.038	300	3.8×10^{-12}
$\Delta H_a = 13 \text{ kcal mol}^{-1}$		$\Delta H = 5 \text{ kcal mol}^{-1}$		$\Delta H = 50 \text{ kcal mol}^{-1}$

Topol, et al., (9) found no evidence for NO_2^+ , by chronopotentiometry, in sodium-potassium nitrate at 280-350°. Also, a thin layer infrared-emission spectrum showed no signs of the NO_2^+ (12). Instead of the self-dissociation proposed by Duke, Topol proposed:



Several papers supporting both sides are referenced in extenso in references 1 and 5. These include discussions of comparisons of results obtained in concentrated sulfuric acid and aqueous systems to those in molten nitrates and nitrites. As the NO_2^+ ion concentration cannot be measured directly, some indirect measurements were reported. Also in one instance the conversion of Mn IV to Mn II was studied. The rates of reaction in molten nitrate were examined under varying conditions. The changes in conditions were the absence or addition of compounds which should cause a change in rate characteristic of one or the other species. The apparent result was the prevalence of NO_2^- over NO_2 as the acid species (13). However, these results are inconclusive, leaving this question still unresolved.

The controversy over the nature of the basic species in molten nitrate is still unresolved. The principal form of oxygen ion, as mentioned earlier, is the center of the dispute. Duke and Kust (8) and Topol, et al., (9) have

tried to establish the species as O^{2-} , while Zambonin and Jordan (10) have supported the O_2^- ion, and have tried to show the nonexistence of the oxide ion.

Topol, et al., (9) have shown the following equilibria to lie to the right:



The equilibrium constant for the alkali metal carbonate reaction was 5×10^{-5} at 300° (14). These equilibria are disputed by Zambonin (15,16,17) as well as by Francini and Martini (18). They believe the only way that these equilibria can lie to the right is by side reactions with water or silica present in either the molten nitrate or from the container used in the studies.

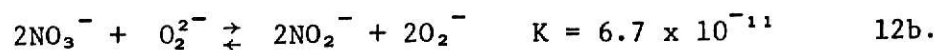
Studies made with an oxygen electrode in molten nitrates have shown differing results. Some researchers (9,14,19,20) have claimed two-electron transfer Tafel slopes corresponding to the equilibrium



while others (10,19,20,21) have obtained one-electron transfer Tafel slopes corresponding to the equilibrium



as proposed by Zambonin and Jordan (10,15,17,21). Zambonin and Jordan (10) proposed three overall equilibria that may exist in the molten nitrate. These equilibria are as follow



The proposed existence of O_2^{2-} and O_2^- at equilibrium has been questioned by Temple, et al., (22) through potentiometric results. They were able to show greater stability for the oxide ion in molten nitrates. Also, Kust (23)

found no signs of peroxide or superoxide in a nitrate melt with added CO_3^{2-} at equilibrium.

To make things even more unclear as to the nature of the basic species some workers (10,19,20,24) have shown other species of oxide ions solvated by nitrate ions:



These species are commonly called orthonitrate, NO_4^{3-} , and pyronitrate, $\text{N}_2\text{O}_7^{4-}$.

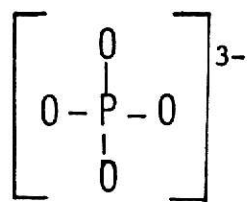
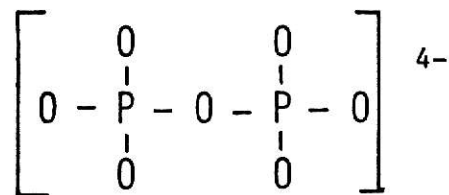
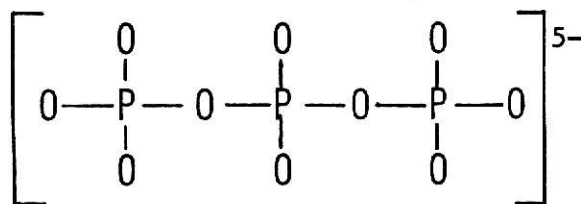
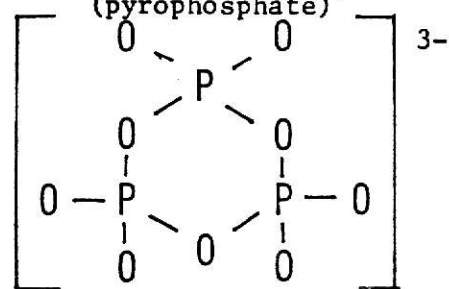
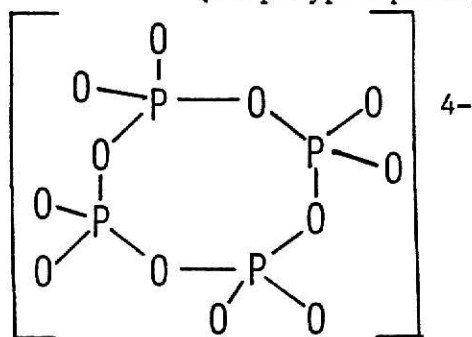
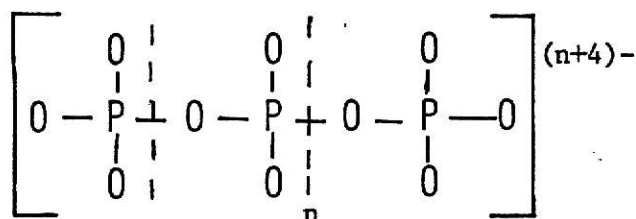
There are many papers concerning the species involved in the acid-base equilibria of molten nitrates, but none are absolutely conclusive. This, for the most part is unimportant to the basic work done in this laboratory. The principal goal here is to study phosphate degradations in molten nitrates, and for this all that is necessary is that the excess molten nitrate solvent functions as a Lux-Flood base. The nitrate anion has been shown to be effective in this capacity (equation 1.).

B. Condensed Phosphates

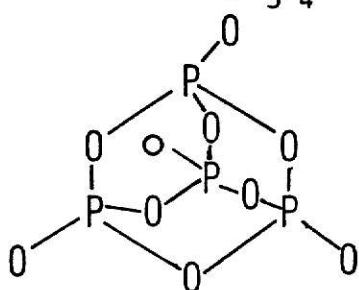
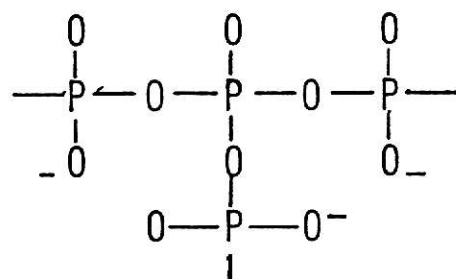
Since 1816 when the first reports of condensed phosphate production were made, the nature of the structures and nomenclature have been the center of much controversy. In depth discussions of the history, structures, properties, reactions, and analysis of the condensed phosphates and the controversies involved have been written by Gutierrez (5), Van Wazer (25), and Emeleus and Sharpe (26).

In this section a brief survey, from the above references, will be made of the currently accepted structures, nomenclature, reactions and methods of analysis, with emphasis on the diphosphate anion, $\text{P}_2\text{O}_7^{4-}$.

The condensed phosphate anions are divided into groups based on structure. Structures ranging from the simple orthophosphate, PO_4^{3-} , to phosphorus (V) oxide are composed of interconnected PO_4 tetrahedra. The groups are chain, cyclic, and ultraphosphates. Fig. 1 shows the structures of some common members of each group. Crystalline forms of members of the cyclic and chain groups have been found. The ultraphosphates however, have never been found

I. orthophosphate, PO_4^{3-} II. diphosphate, $\text{P}_2\text{O}_7^{4-}$
(pyrophosphate)III. triphosphate, $\text{P}_3\text{O}_{10}^{5-}$
(tripolyphosphate)IV. trimetaphosphate
 $(\text{PO}_3)_3^{3-}$ V. tetrametaphosphate
 $(\text{PO}_3)_4^{4-}$ 

VI. classical "metaphosphate"

VII. phosphorus "pentoxide"
 P_4O_{10} 

VIII. ultraphosphate

Fig. 1.. Structures of several typical condensed phosphate anions.

in the crystalline form. These phosphates have been shown to exist in glasses obtained from phosphate melts above 350°. These ultraphosphates are also called branching point structures because of the mutual sharing of three oxygens of a PO_4 tetrahedron to form the interconnected structure.

The PO_4 tetrahedron exhibits sp^3 hybridized bonding by the phosphorus atom. The "metaphosphates" are denoted by a structure of empirical formula $(\text{PO}_3)_n^{n-}$ where the PO_4 tetrahedra are joined through single oxygen atoms and are thus cyclic in structure. Values of n from 3 to 6 have been justified with some belief that structures with values of $n = 7$ and 8 exist. Two common forms of "metaphosphates" are IV and V of Fig. 1. The chain phosphate anions, I, II, and III of Fig. 1, have a structure of empirical formula $(\text{P}_n\text{O}_{3n+1})^{(n+2)-}$. This series has been characterized up to hexapolyphosphate, or an n value of 6. Another member of this group is the chain or classical metaphosphate whose basic structure is shown by VI in Fig. 1. These so-called metaphosphates are the ultimate in the series.

Quantitative analysis of condensed phosphate mixtures relies mostly on paper chromatography, nuclear magnetic resonance spectroscopy, and infrared spectroscopy. The use of paper chromatography is limited to mixtures of meta- and polyphosphates with chain lengths of $n = 1$ -10. This method is the most reliable. Infrared spectroscopy is limited to crystalline samples of mixed phosphates. Nuclear magnetic resonance spectroscopy is probably the simplest method for determination of phosphate structures and concentrations in mixtures, but it is practically limited to chain lengths of four P atoms because of signal overlap.

The P atom of H_3PO_4 exhibits the greatest amount of deshielding by the oxygen atoms, and thus this is used as the usual reference for nmr spectroscopy of mixtures of phosphorus containing compounds. The signal from a solution of 85% H_3PO_4 is used as zero ppm on nmr spectra. Moving upfield to a zone of less deshielding (+4 to +12 ppm) one finds the end group region where P atoms of PO_4 tetrahedra have three terminal oxygen atoms rather than four. Signals in this region arise, for example from the P atoms of the diphosphate anion, $\text{P}_2\text{O}_7^{4-}$, shown in II of Fig. 1, and the P atoms of the two end PO_4 tetrahedra of triphosphate anion, $\text{P}_3\text{O}_{10}^{5-}$, shown in III of Fig. 1. Moving still further

upfield to a zone of even less deshielding (+18 to +23 ppm) one finds the middle group PO_4 tetrahedra signals. These middle groups have only two terminal oxygen atoms on a PO_4 tetrahedron, the remaining two atoms being involved in bridging. Such PO_4 tetrahedra exist, for example, in the structures of cyclic metaphosphates and the middle PO_4 group in the triphosphate anion. These structures are illustrated in IV, V, and III of Fig. 1, respectively.

Diphosphate (or pyrophosphate) anion, $\text{P}_2\text{O}_7^{4-}$, is of the greatest importance to this work. It gives rise to a single end group type nmr signal at approximately +6 ppm from H_3PO_4 . Diphosphate, like many condensed phosphates, is produced by thermal treatment of sodium monohydrogen orthophosphate to form the condensed phosphate and eliminate water. The crystal structure of $\text{Na}_4\text{P}_2\text{O}_7 \cdot 10 \text{H}_2\text{O}$ shows that the diphosphate anion is made up of two PO_4 tetrahedra joined through a common oxygen atom in what appears to be a trans configuration. The P-O-P angle is about 134° , and the P-O bond length of the P-O-P bridge is greater than that of the P-O terminal bonds.

The condensed phosphates described above are excellent choices as Lux-Flood acids. These phosphates are degraded in the presence of an oxide ion donor or a free oxide ion. This degradation results in the rupturing of the P-O-P bridges and addition of O^{2-} . The extent of this degradation is affected by not only the Lux-Flood base but also by the associated cations.

Potentiometric determinations of relative acidities and basicities were found for several phosphates and oxide containing bases (19,27). Titrations of the acids (phosphates) dissolved in an inert molten electrolyte were made using different bases. The end point of neutralization was determined by a drop in potential of an oxygen electrode, from steady state. The study of the titration of sodium metaphosphate (believed to be trimeta-, but represented as NaPO_3), using different bases in different solvents, was of most importance. It was found that using the same base but different molten electrolytes gave a variety of final degradation products.

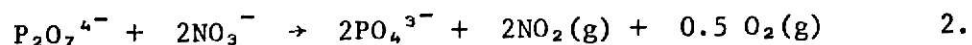
Titration of the metaphosphate with Na_2O_2 , using an electrolyte solvent of LiCl-KCl eutectic, resulted in a one-step neutralization yielding a final product of diphosphate, $\text{P}_2\text{O}_7^{4-}$. However, if the electrolyte was changed to KNO_3 , another step in the neutralization appeared, following the previous step. This was the degradation of the diphosphate anion to orthophosphate anions. This shows the varying effect of different electrolytes. It was also found that different bases yielded different degradation products. Na_2O_2 gave a

two-step process of neutralization for the metaphosphate: first to diphosphate, then to orthophosphate. However, in the same electrolyte, KNO_3 , any of the bases: CO_3^{2-} , HCO_3^- , HCOO^- , $(\text{COO})_2^{2-}$, or CH_3COO^- , gave a three-step neutralization: first to triphosphate, III of Fig. 1, then to diphosphate, and finally to orthophosphate. In a further study of the metaphosphate degradation the alkali metal of the salt was varied, yielding another effect on the outcome of the degradation. The oxide source was the corresponding alkali metal perchlorates, MClO_4 . The results of the study were complete degradation of the metaphosphates to orthophosphate using lithium cations, and the metaphosphates to diphosphate, using sodium and potassium cations.

Thus, relative acidities were determined for the di- and metaphosphate: first, with a given cation as a function of the bases used, and then as a function of the associated cations. The metaphosphate was found to be a stronger acid than diphosphate with a given cation. As for the associated cations of the metaphosphate, lithium was found to be more greatly acidic than sodium, which was slightly more acidic than potassium. The diphosphate acidities, based on the associated cations, showed that lithium increased acidity while sodium and potassium had no effect. This results in no degradation of $\text{P}_2\text{O}_7^{4-}$ in the presence of these last two cations. As will be pointed out in further detail in the next section, the degradation of diphosphate anion in excess molten nitrates is first order in diphosphate, and only occurs if a lithium-containing molten nitrate solvent is used.

C. Solvolytic Scission of the Diphosphate Anion By Molten Lithium Nitrate

Gutierrez (5) found that the final degradation product of condensed phosphate anions, whether chain or cyclic, was the diphosphate anion when only sodium salts were used. However, when he used LiNO_3 instead of NaNO_3 as the solvent the trimetaphosphate was degraded to PO_4^{3-} . In the summer of 1974 Hubble continued the investigation concerning a Li^+ cation effect. He observed that, like the trimetaphosphate anion, the diphosphate anion was also degraded to the orthophosphate anion in molten lithium nitrate. The reaction was



ILLEGIBLE


**THE FOLLOWING
DOCUMENT(S) ARE
OF POOR
LEGIBILITY DUE
TO STAINS AND OR
WATER DAMAGE**

ILLEGIBLE

The reaction was carried out in an excess of lithium nitrate (55:1 mole ratio LiNO_3 to $\text{Na}_4\text{P}_2\text{O}_7$). Hubble obtained kinetics for this reaction at four temperatures from 610 to 625°K. The reaction was found to be first order with respect to the diphosphate anion. Quenched samples were obtained at various times at each temperature. The solid samples were prepared for ^{31}P nmr analysis by dissolution in distilled water acidified to pH of 3. This acidification was necessary to facilitate dissolution. Since hydrolytic scission of the diphosphate anion is a common reaction, the question of the occurrence of this reaction arose. Hubble made a study of a blank solution of 55:1 mole ratio $\text{LiNO}_3:\text{Na}_4\text{P}_2\text{O}_7$, that had been acidified to pH = 3. The ^{31}P nmr spectra of this blank at different times over a month showed that the first order hydrolysis half life was ca. 194 days, or 6 months. This was obtained from a natural logarithm plot of the fraction of unreacted $\text{P}_2\text{O}_7^{4-}$ versus time. The fraction of diphosphate was calculated from the integrated intensities of the ortho- and diphosphate signals in the nmr spectra. The calculation was done by finding the area under each peak with a planimeter, and then using the following equation for the fraction of unreacted $\text{P}_2\text{O}_7^{4-}$, X_{DP} :

$$X_{\text{DP}} = (\text{Area } \text{P}_2\text{O}_7^{4-} / 2) / [(\text{Area } \text{P}_2\text{O}_7^{4-} / 2) + \text{Area } \text{PO}_4^{3-}] \quad 14.$$

It was also found that no orthophosphate existed on the first day. Thus, Hubble was able to conclude that if spectra were obtained soon after the dissolution of the residue, any orthophosphate present would have occurred only from the reaction of $\text{P}_2\text{O}_7^{4-}$ with molten LiNO_3 .

In Table 2 the data obtained by Hubble are found, with the rate constants, k_1 . In Fig 2 the plots of the natural logarithm of the fraction of unreacted $\text{P}_2\text{O}_7^{4-}$, \ln , versus time, t (min), at the different temperatures are shown. The rate constants, k_1 , were obtained by taking the least squares slopes, forcing the lines through the origin (28). The least squares straight line from an Arrhenius plot of $\ln k_1$ versus $1/T$ ($^\circ\text{K}$) $^{-1}$ is:

$$\ln k_1 = (30.35 \pm 3.11) - (1.97 \pm 0.24) \times 10^4 (1/T) \quad 15.$$

where the errors are probable errors. This is based on the equation (29):

$$k_1 = A \exp(-E_a/RT) \quad 16.$$

The energy of activation was calculated as $E_a = (164.07 \pm 23.67) \text{ kJ mol}^{-1}$ ($39.21 \pm 5.66 \text{ kcal mol}^{-1}$). The activation entropy, ΔS^\ddagger , was calculated from the intercept of the Arrhenius plot as $\Delta S^\ddagger = (-40.77 \pm 38.33) \text{ J/}^\circ\text{K mol}$ ($-9.75 \pm 9.16 \text{ e.u. mol}^{-1}$) for $T = 600^\circ\text{K}$. This calculation is based on:

$$\ln A = \ln (ekT/h) + \Delta S^\ddagger/R \quad 17.$$

which is a result of

$$A = (ekT/h) \exp(\Delta S^\ddagger/R) \quad 18.$$

The reaction of $\text{P}_2\text{O}_7^{4-}$ in molten LiNO_3 can be regarded as a solvolysis reaction (30). A comparison can be made between this reaction and the hydrolytic scission of the diphosphate anion (6). In the former, Li^+ is the catalyst, and in the latter it is H^+ . Comparison of these reactions can be further supported by observing the activation energies and activation entropies. For the hydrolysis of diphosphate in a strongly acid solution the activation energy and activation entropy are $E_a \sim 15\text{--}16 \text{ kcal mol}^{-1}$ and $\Delta S^\ddagger \sim -30 \text{ e.u. mol}^{-1}$, respectively (6). On the other end of the scale, for reactions occurring in weakly acidic through neutral to pH 10 solutions, these values are $E_a \sim 30\text{--}40 \text{ kcal mol}^{-1}$ and $\Delta S^\ddagger \sim -5 \text{ to } -1 \text{ e.u. mol}^{-1}$ (6). Comparison of these values with those mentioned previously for the Li^+ catalyzed reaction shows that values for the weakly acidic to pH = 10 solutions are of similar magnitude.

It is believed that the two different pH conditions for the hydrolysis reaction are characterized by individual mechanisms. These are thought to be S_N2 in strong acid solution and S_N1 in weakly acidic to pH = 10 (6,31). At ca. pH = 4 the proposed S_N1 mechanism is believed to involve the dissociation of $\text{H}_2\text{P}_2\text{O}_7^{2-}$ into PO_4^{3-} and PO_3^- as the rate controlling step (6,31). The PO_3^- would rapidly undergo nucleophilic attack by the solvent, H_2O .

Chain phosphates, such as diphosphate, are known to complex metal ions. Alkali metals are complexed by the chain phosphates not only in aqueous solutions but apparently in melts as well (25). Nearly 100% ionic character is associated with the complex bonds of the alkali metal cations (25). The effect of this complex formation is seen in ^{31}P nmr spectra, which exhibit no chemical shift but do display an abnormal lowering and spreading of the intensity (25).

Table 2. Summary of residual $P_2O_7^{4-}$ content at various times at 337, 342, 347, and 352°, first order rate constants, and activation energy and entropy for the $LiNO_3$ (xs) + $Na_4P_2O_7$ reaction

Reaction time, t, min	Fraction of total P in residue as $P_2O_7^{4-}$, X_{DP}	$-\ln X_{DP}$	Rate constant, ^a k_1 , min ⁻¹
337°			
0	1.000	0	$14.23 \pm .22 \times 10^{-2}$
3.0	0.620	0.47742	
4.0	0.537	0.62140	
5.0	0.427	0.84992	
7.0	0.342	1.07232	
10.0	0.255	1.36828	
12.0	0.198	1.62080	
342°			
0	1.000	0	$16.27 \pm .30 \times 10^{-2}$
2.0	0.737	0.30517	
3.5	0.538	0.61990	
5.0	0.391	0.93905	
5.5	0.386	0.95192	
7.0	0.289	1.24133	
10.0	0.201	1.60445	
12.0	0.162	1.82016	
347°			
0	1.000	0	$22.63 \pm .35 \times 10^{-2}$
3.0	0.477	0.74024	
4.0	0.414	0.88189	
5.0	0.329	1.11170	
6.0	0.262	1.33941	
7.0	0.184	1.69282	
9.0	0.140	1.96611	

Table 2, continued

Reaction time, t, min	Fraction of total P in residue as $P_2O_7^{4-}$, X_{DP}	$-\ln X_{DP}$	Rate constant, ^a k_1 , min^{-1}
352°			
0	1.000	0	
2.0	0.541	0.61434	
2.5	0.448	0.80296	
3.0	0.439	0.82326	
3.5	0.373	0.98618	
4.0	0.281	1.26940	$(30.23 \pm .77) \times 10^{-2}$
4.5	0.192	1.65026	
5.0	0.207	1.57504	
5.5	0.158	1.84516	
6.0	0.196	1.62964	
7.0	0.147	1.91732	

$$E_a = 164.07 \pm 23.67 \text{ kJ mol}^{-1} \quad (39.21 \pm 5.66 \text{ kcal mol}^{-1})^b$$

$$\Delta S^\ddagger = -40.77 \pm 38.33 \text{ J K}^{-1} \text{ mol}^{-1} \quad (-9.75 \pm 9.16 \text{ e.u. mol}^{-1})^b$$

$$E_a = 158.93 \pm 15.94 \text{ kJ mol}^{-1} \quad (37.99 \pm 3.81 \text{ kcal mol}^{-1})^c$$

$$\Delta S^\ddagger = -49.33 \pm 25.81 \text{ J K}^{-1} \text{ mol}^{-1} \quad (-11.79 \pm 6.17 \text{ e.u. mol}^{-1})^c$$

^a Errors given for k_1 values, and for E_a and ΔS^\ddagger , are probable errors.

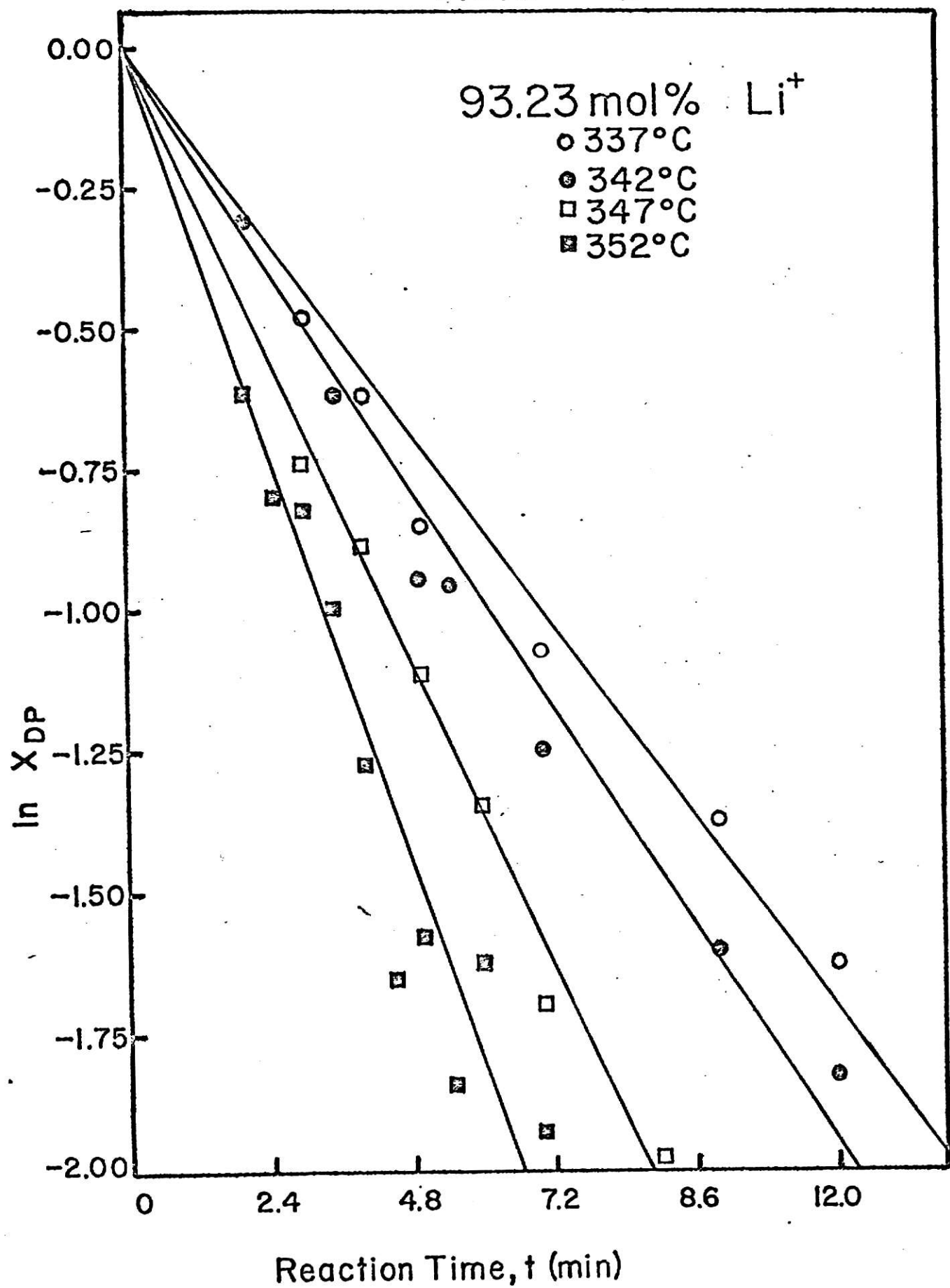
^b Computed from a plot of $\ln k_1$ versus $1/T$ using $T = 600^\circ\text{K}$ for ΔS^\ddagger . This plot is shown in Fig. 13.

^c Computed from a plot of $\ln (k_1/T)$ versus $1/T$. This plot is shown in Fig. 14.

Explanation of Plate I.

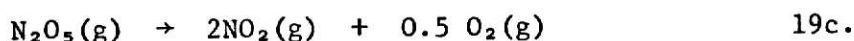
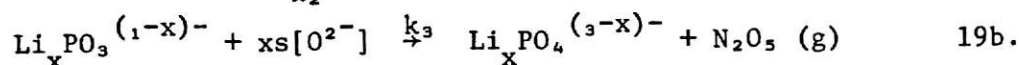
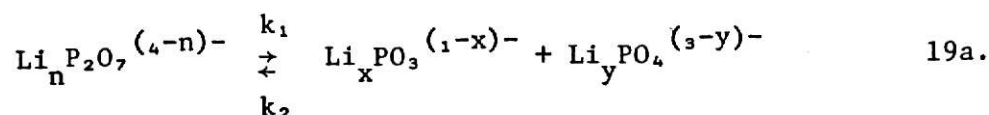
Fig. 2. Plots of Hubble's data of the natural logarithm of the fraction of phosphorus remaining as $P_2O_7^{4-}$, $\ln X_{DP}$, versus time, t (min), at various temperatures for the reaction of $P_2O_7^{4-}$ with excess molten $LiNO_3$, where the cation mole percent of Li^+ is 93.23 mol %.

Plate I



Electrophoresis measurements also support bonding of alkali metal cations with the chain phosphates, with Li^+ being the strongest (25).

The $\text{S}_{\text{N}}1$ type mechanism that has been proposed to interpret Hubble's work is:



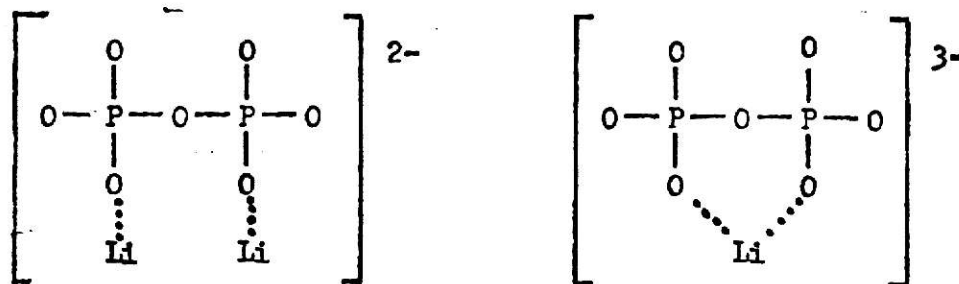
where the first step is a Li^+ -catalyzed dissociation of $\text{P}_2\text{O}_7^{4-}$, and the second step is a nucleophilic attack on the monometaphosphate, PO_3^- , by excess $[\text{O}^{2-}]$, where $[\text{O}^{2-}]$ represents the effective donation of oxide ion from the nitrate. The upper limit to n would be 4, while $x + y = n$. The rate law for such a mechanism is:

$$\frac{d[\text{Li}_n\text{P}_2\text{O}_7^{(4-n)-}]}{dt} = \frac{-k_1 k_3 [\text{Li}_n\text{P}_2\text{O}_7^{(4-n)-}] [\text{O}^{2-}]}{k_2 [\text{Li}_x\text{PO}_3^{(1-x)-}] + k_3 [\text{O}^{2-}]} \quad 20.$$

which, if the rate of the second step is much greater than that of the first ($k_3 [\text{O}^{2-}] \gg k_2$), reduces to (32)

$$\frac{d[\text{Li}_n\text{P}_2\text{O}_7^{(4-n)-}]}{dt} = -k_1 [\text{Li}_n\text{P}_2\text{O}_7^{(4-n)-}] \quad 21.$$

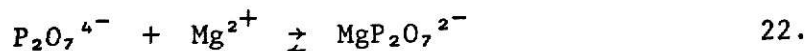
Hubble used this rate expression, substituting the fraction of unreacted diphosphate, X_{DP} , for the concentration of $[\text{Li}_n\text{P}_2\text{O}_7^{(4-n)-}]$. The dissociation is believed to occur because Li^+ weakens the P-O-P bridge via strong electron withdrawing interactions due to coordination of the Li^+ cation to terminal oxygens. Two possible structures proposed for the species which dissociates, $\text{Li}_n\text{P}_2\text{O}_7^{(4-n)-}$, were



I

II

Species (I) would be analogous to the $\text{H}_2\text{P}_2\text{O}_7^{2-}$ (6) protonated species occurring at ca. $\text{pH} = 4$, as mentioned earlier. Species (II) is justified to its possible existence by lithium's propensity to assume a double coordination number (e. g. as with acetylacetonate) (33). Also, a species such as (II) has already been postulated as being involved in hydrolytic scission of low molecular weight chain phosphates (34). Species (II) could not have more than one Li^+ cation coordinated across the P-O-P bridge because of its bond angle which is accepted as ca. 134° . These Li^+ coordinated complexes can to some extent be demonstrated by nmr. As mentioned before, a lowering and spreading in intensity of the complexed peak is observed. Hubble observed this lowering and spreading in the diphosphate peak, while Gutierrez observed no such lowering in reactions in molten NaNO_3 (5,7). Also, it has been shown by nmr that Mg^{2+} , which is similar to Li^+ , forms a complex with $\text{P}_2\text{O}_7^{4-}$ in aqueous solution,



with a lifetime of less than 10^{-2} sec with respect to uncomplexed diphosphate (35).

D. Hydrolysis of the Diphosphate Anion as a Function of pH.

As stated previously, hydrolysis of the diphosphate anion results in formation of orthophosphate anions. Osterheld has combined several studies of the above hydrolysis into a survey of nonenzymatic hydrolysis of condensed phosphates (6). Some of the results of this have been discussed in the last

section. As the present work deals with the rate of solvolytic scission as a function of the lithium cation concentration, it is felt that a small section dealing with hydrolytic scission as a function of pH, or hydrogen cation concentration, is appropriate.

Fig. 3 contains Arrhenius plots of the logarithm of the first order rate constants versus $10^3/T(^{\circ}\text{K})^{-1}$ (6). Dashed lines are the results of work which

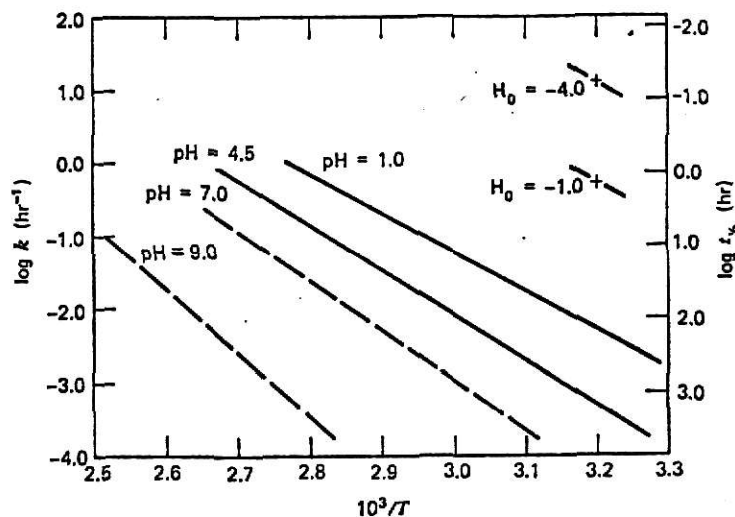


Fig. 3. Plots of the common logarithm of the first order rate constants, $\log k_1$, versus $1/T (^{\circ}\text{K})^{-1}$ for the hydrolysis of $\text{P}_2\text{O}_7^{4-}$ at various pH's (6).

showed a higher degree of scattering, believed to be caused by cations other than the hydrogen ion being present. The plots of Fig. 3 show that an increase in pH is associated with an increase in the activation energy of the reaction. This follows the idea of the hydrogen ion being in the role of a catalyst in the reaction.

Fig. 4 contains plots of the common logarithm of the first order rate constants, $\log k_1 (\text{hr}^{-1})$, versus pH (6). Here it can be seen that a plateau is reached in all cases at approximately pH = 4. The dashed lines are based on few experimental points. Curve (a) is for the hydrolysis of a diphosphate ester. This curve has a second plateau starting at an approximate pH of 10.

An interpretation of the change in rate of hydrolysis with pH is the change in relative abundance of the various protonated diphosphate species.

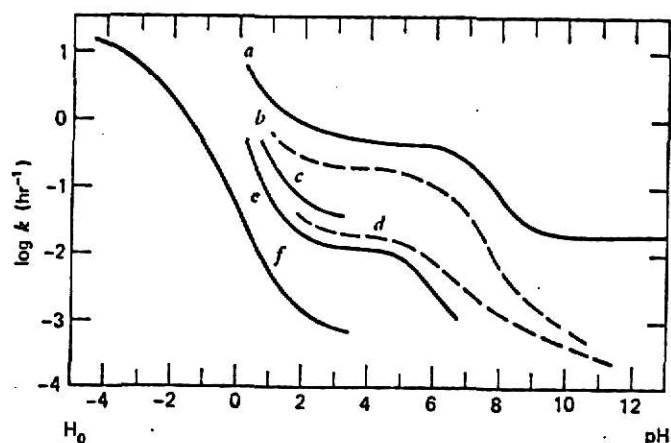


Fig. 4. Plots of the common logarithm of the first order rate constants, $\log k_1$ (hr^{-1}), versus pH for the hydrolysis of the diphosphate anion. Curve (a) is for γ -phenylpropyl diphosphate at 95° . Remaining curves are for inorganic diphosphate at (b) 90° ; (c) 69° ; (d) 65.50° ; (e) 60° ; and (f) 40° (6).

The evidence for this idea comes from the curves of Fig. 4. At low pH the expected species would be $\text{H}_4\text{P}_2\text{O}_7$, at pH = 4 the species in abundance is $\text{H}_2\text{P}_2\text{O}_7^{2-}$, and at high pH values the species present in solution is $\text{P}_2\text{O}_7^{4-}$. Fig. 4 shows that the rate constants decrease as pH increases. Thus, it appears that the change in rate is due to a change in form of protonated species present in solution. Curve (a) further supports this idea in that the curve is for the hydrolysis of a diphosphate ester, $\text{RH}_3\text{P}_2\text{O}_7$. In this curve there are two plateaus, the first corresponding to those of the other curves at pH = 4, and the second at a pH = 10. The first plateau could possibly be due to a doubly protonated species, $\text{RH}_2\text{P}_2\text{O}_7^{1-}$, and the second plateau to a third ionic species, $\text{RP}_2\text{O}_7^{3-}$. Since the ester cannot attain the complete $\text{P}_2\text{O}_7^{4-}$ state, like an inorganic diphosphate, it reaches this last plateau at about pH = 10, and the rate does not change for hydrolysis at higher pH's. It is known that the only species of inorganic diphosphate in abundance (other than $\text{P}_2\text{O}_7^{4-}$) over an extended pH range in basic solution is $\text{H}_2\text{P}_2\text{O}_7^{2-}$. Thus, the reasoning behind the change in form of protonated species accounting for the effect of different pH solutions seems to be plausible.

EXPERIMENTAL

I. Chemicals

The effect of varying the LiNO_3 to NaNO_3 mole ratio on the degradation of $\text{Na}_4\text{P}_2\text{O}_7$ was studied. Reagent grade $\text{Na}_4\text{P}_2\text{O}_7 \cdot 10 \text{ H}_2\text{O}$ was obtained from Baker and Adamson Co. This salt was thermally and quantitatively dehydrated by placing it in a porcelain casserole and then heating with a burner for ca. 2 hours, then oven drying for 72 hours at 130° (36). The LiNO_3 in reagent grade was obtained from Fisher Scientific Co. This salt was vacuum dried at 120° for ca. 48 hours (5). The LiNO_3 and $\text{Na}_4\text{P}_2\text{O}_7$ were transferred to a drybox where each was finely ground by mortar and pestle. Reagent grade NaNO_3 was obtained from Mallinckrodt Co. This salt was dried for at least 24 hours in an oven at 125° (5,7). It was thoroughly ground by mortar and pestle and placed in the drybox. All the above compounds were handled in a drybox during the process of weighing, and were removed in sealed reaction vessels for the kinetic runs.

Argon was obtained from the National Cylinder Gas Co., and had a stated purity of 99.9%. This gas was passed through a drying tower containing CaSO_4 before entering the kinetic reaction vessels as a purging gas. Nitrogen was also obtained from the National Cylinder Gas Co. and was used for the atmosphere of the drybox after the gas was passed through a drying tower of 4-8 mesh molecular sieves, Type 5A from Fisher Scientific Co.

II. Apparatus

A. Constructed Apparatus

For the kinetic runs a vessel such as that in Fig. 5 was used (37). This vessel was first introduced by Gutierrez (5). It consisted of a 25 x 200 mm Vycor testtube as the outer jacket, A. The inner jacket, B, consisted of 12 mm o.d. Pyrex tube, 20 cm in length. This inner jacket was charged with phosphate through an opening, C. The innermost tube, (called the plunger) D, was a 3 mm o.d. Pyrex tube, open throughout and terminated at the bottom by a

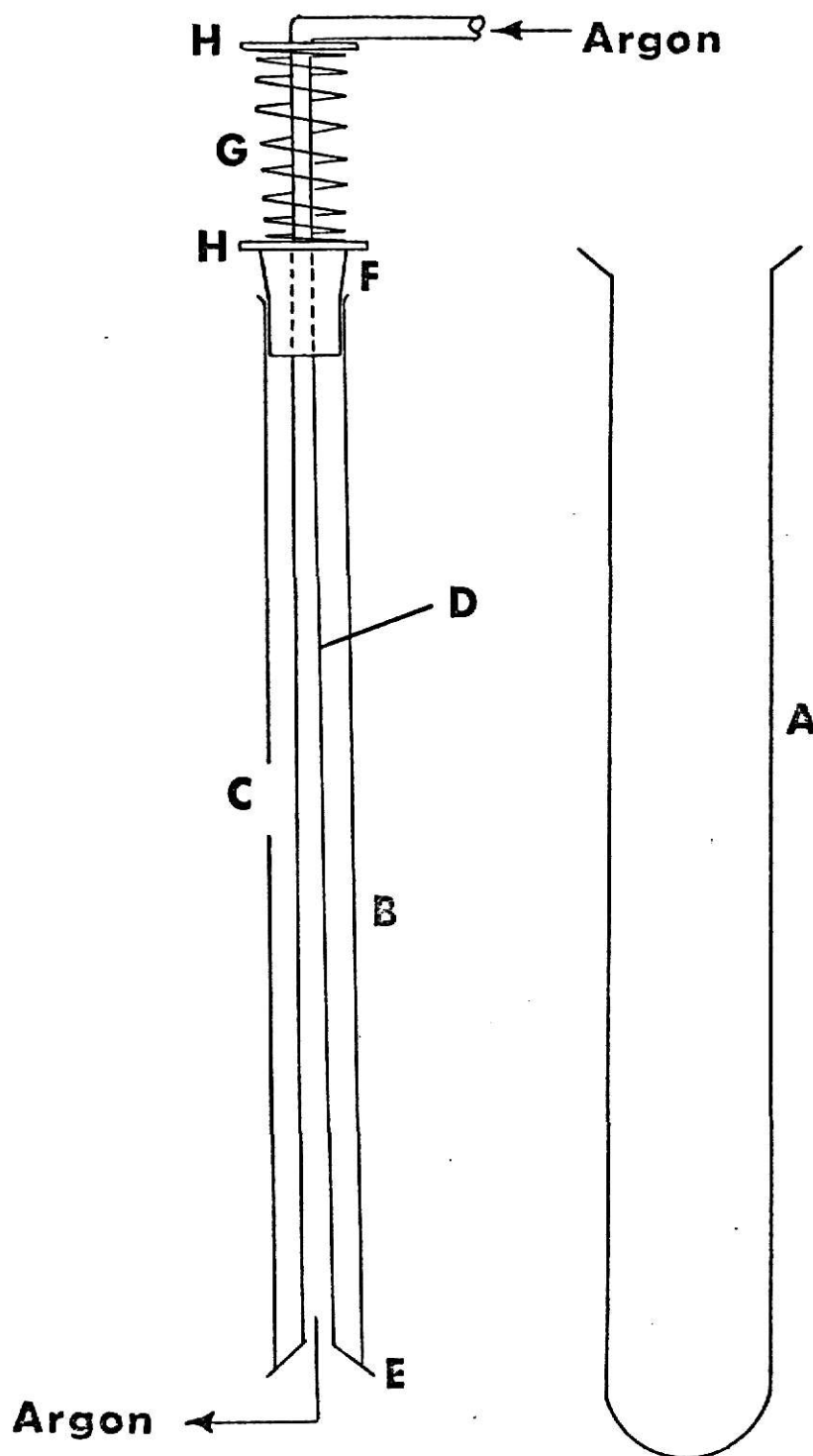


Fig. 5. Quenched reaction vessel. A and B are the outer and inner jackets, respectively. D is the innermost glass tube, (called the plunger), G is a metal spring, F is a cork, E is the beveled flange, C is an entrance opening for charging the inner jacket with the diphosphate reactant, and H represents the metal washers.

beveled flange, E. The beveled flange was held against the bottom of the inner jacket, B, by a bored number 3 cork, F, and a metal spring, G, fixed between two metal washers, H. The inner jacket extended to within 4 cm of the bottom of the outer jacket, and was held in place by a bored number 9 cork.

A high temperature bath, with molten NaNO_3 - KNO_3 eutectic as the liquid, was constructed to maintain a constant temperature in these kinetic studies. The form is the same as that employed by Gutierrez (5) and Hubble in their work. It consisted of a cylindrical metal-porcelain container 28 cm in diameter, and 20 cm in depth, and was provided with a 9.5-mm Transite sheet cover. The container was wrapped with several layers of asbestos paper, and was further insulated with fire brick. These bricks were type A-20 from Armstrong Cork Co. A final layer of asbestos paper was placed over the fire brick. The asbestos paper and fire brick were held in place by wire. The NaNO_3 was reagent grade from the J. T. Baker Co., while KNO_3 was also reagent grade from Mallinckrodt Co. The purity of these salts was needed to maintain a clean liquid in the bath. The entire assembly was placed on a Scientific Co. hot plate whose temperature was controlled by a 220-V powerstat and a 0-30 A a.c. ammeter. Four holes, each 26 mm in diameter, were drilled through the Transite cover to allow insertion of the reaction vessels. Two smaller holes were drilled in the Transite cover, one about 5 cm from the side of the cylindrical container to permit insertion of a Pyrex rod stirrer, which was operated by a Precision Scientific Co. (Cat. Number 65748A) 220-V variable rotator. The other small hole, about 3.5 cm from the side, was for the insertion of a 7 mm o.d. Pyrex sheath. A chromel-alumel thermocouple was placed in this sheath to monitor the temperature. The sheath extended to within 2.5 cm of the bottom of the container.

B. Commercial Apparatus

The thermocouple used in temperature measurements was made of Leeds and Northrup Company 24-gauge pre-calibrated Chromel (Cat. Number 57892-15) and Alumel (Cat. Number 35264-5) wires. All high temperature monitoring was done with the leads of the chromel-alumel thermocouple connected via an ice-bath reference junction to a Leeds and Northrup Company Number 8691 millivolt potentiometer (error of $\pm 0.5^\circ$).

A Lab-line Instruments Incorporated Lab-chron 1400 timer was used to monitor the elapsed time in the kinetic runs.

A Varian Associates XL-100 nmr spectrometer was employed to obtain the ^{31}P nmr spectra at 40.5 MHz. Spectra were accumulated with a Varian Associates C-1024 Time Averaging Computer (CAT). The lock signal used was a proton lock (H_2O). Samples were contained in Wilmad Glass Company 12 mm o.d. nmr sample tubes equipped with the usual tight-fitting plastic caps.

All handlings of the chemicals were done in a Lab Con Company drybox, except for the kinetic runs themselves.

All weighings were made using a Mettler Instrument Corporation Model H6 balance.

All integrations of nmr spectra were made using a K and E Compensating Planimeter.

III. Quenched Reaction Kinetic Studies

A. 70-30 mol % LiNO_3 - NaNO_3

The procedure was the same as that employed by earlier workers (5). In a drybox, 1.0005 g of LiNO_3 , 0.5270 g of dry NaNO_3 , and 0.1000 g of $\text{Na}_4\text{P}_2\text{O}_7$ were weighed. These masses represented a 55:1 mole ratio of $\text{NO}_3^-:\text{P}_2\text{O}_7^{4-}$, and a 70:30 mole ratio of $\text{LiNO}_3:\text{NaNO}_3$. The LiNO_3 and NaNO_3 were placed in the outer jacket of the reaction vessel (A of Fig. 5). The $\text{Na}_4\text{P}_2\text{O}_7$ was placed in the inner jacket of the vessel (B of Fig. 5). Three of these vessels were placed at one time in the high temperature bath to within 3 cm of the bottom. Argon was constantly passed through each reaction vessel while it was coming to equilibrium at the desired temperature. This temperature was determined by the chromel-alumel thermocouple. The argon flow rate was $20\text{--}25\text{ cm}^3\text{ min}^{-1}$. When the vessel and contents had reached equilibrium at the desired temperature, the argon flow was terminated and the plunger of the inner jacket (D of Fig. 5) was depressed to allow the $\text{Na}_4\text{P}_2\text{O}_7$ to drop into the molten nitrate solvent. Timing was begun immediately, during the first 1-2 min of which the system was manually agitated to facilitate the dispersion and dissolution of the solid $\text{Na}_4\text{P}_2\text{O}_7$ into the molten nitrate. The reaction was terminated by plunging the reaction vessel into an ice bath. The vessel was then flushed with argon. The inner jacket was removed, and the outer jacket was stoppered

and stored for later residue analysis. A series of 6 or 7 quenched reactions were made at different times, constituting a run, and a run was obtained at temperatures of 337, 342, 347, and 352°.

Dissolution of the reaction residues in deionized water, for ^{31}P nmr analysis, was performed in the same manner as in previous studies (5,7). The residue was dissolved in ca. 10 cm³ of deionized water acidified with 3 drops of concentrated hydrochloric acid, which gave the solutions a pH of approximately 3. The spectra were obtained within 3 to 7 hours after the solutions were prepared. As was pointed out previously Hubble found that spectra obtained during the first day showed no signs of any orthophosphate, other than that from reaction with nitrate.

As nmr peaks arose only for PO_4^{3-} and $\text{P}_2\text{O}_7^{4-}$, it was not necessary to include a capillary of 85% H_3PO_4 as a standard, as was the case in other works (5,7). The phosphorus content of both species was determined by integrating the intensities of the respective peaks. This was accomplished by measuring the area under the peaks with a K and E Compensating Planimeter. Calculation of the fraction of unreacted diphosphate was done using equation 14:

$$X_{\text{DP}} = (\text{Area } \text{P}_2\text{O}_7^{4-} / 2) / [(\text{Area } \text{P}_2\text{O}_7^{4-} / 2) + \text{Area } \text{PO}_4^{3-}] \quad 14.$$

The fraction of unreacted diphosphate, X_{DP} , was calculated in this manner because the total area of both peaks represents the total phosphorus content. However, the diphosphate peak area represents the phosphorus atoms in $\text{P}_2\text{O}_7^{4-}$ rather than the number of molecules. Thus, division of the $\text{P}_2\text{O}_7^{4-}$ area by 2 is necessary to correct for this.

B. 80-20 mol % LiNO_3 - NaNO_3

The procedure was the same as in part A above except that the mole ratio of LiNO_3 : NaNO_3 was changed to 80:20. A mole ratio of 55:1 for the NO_3^- : $\text{P}_2\text{O}_7^{4-}$ was still maintained. The masses used were 1.1385 g LiNO_3 , 0.3570 g NaNO_3 , and 0.1000 g $\text{Na}_4\text{P}_2\text{O}_7$. Nmr analyses again were used to determine the unreacted diphosphate fractions, X_{DP} . The runs were made at the same temperatures: 337, 342, 347, and 352°.

C. 90-10 mol % LiNO_3 - NaNO_3

Again everything was the same as in part A except that the ratio of LiNO_3 : NaNO_3 was 90:10. The masses were 1.2834 g LiNO_3 , 0.1785 g NaNO_3 , and 0.1000 g $\text{Na}_4\text{P}_2\text{O}_7$. Nmr analyses were used as before to find the fraction of unreacted diphosphate. A run was made at each of the following temperatures: 337, 342, 347, and 352°.

RESULTS AND DISCUSSION

Tables 3 through 8 contain results of the quenched reaction kinetic studies of the $\text{Na}_4\text{P}_2\text{O}_7$ - LiNO_3 reaction. The reaction consisted of the decomposition of $\text{P}_2\text{O}_7^{4-}$ and the formation of PO_4^{3-} . A typical ^{31}P nmr spectrum is shown in Fig. 6 for a quenched sample after 15 min in the 342° run with a Li^+ cation mole percent of 74.31 mol %. The broad peak at about 10.4 ppm is the signal from the phosphorus atoms of $\text{P}_2\text{O}_7^{4-}$ and the sharper peak at 0 ppm is the signal from the phosphorus atoms of PO_4^{3-} .

The $\text{Na}_4\text{P}_2\text{O}_7$ - LiNO_3 reaction was studied at 337 , 342 , 347 , and 352° at various mole percentages of LiNO_3 . The mole percent was controlled by the variance of the mole ratio of LiNO_3 to NaNO_3 . This was due to the inertness of $\text{Na}_4\text{P}_2\text{O}_7$ in molten NaNO_3 previously substantiated by Gutierrez (5). The ratio of NO_3^- to $\text{P}_2\text{O}_7^{4-}$ was always maintained at 55 to 1, and the mole ratio of LiNO_3 to NaNO_3 was 70 to 30, 80 to 20, and 90 to 10 (and 100 to 0 from Hubble's work). However, since the Li^+ cation was the catalyst for the reaction, the cation mole percent of Li^+ was what was actually needed. Thus, the total moles of Na^+ from both $\text{Na}_4\text{P}_2\text{O}_7$ and NaNO_3 in the liquid system had to be considered when calculating the actual cation mole percent of Li^+ . The actual cation mole percentages of Li^+ studied were thus 65.30, 74.31, and 83.77 mol % (and 93.23 mol % from Hubble's work). The data are arranged according to cation mole percent of Li^+ . For each mole percentage the data are further divided according to the temperatures of the runs.

Tables 3 through 8 also contain reaction times, t (min), at which samples were quenched, areas of $\text{P}_2\text{O}_7^{4-}$ peaks, areas of $\text{P}_2\text{O}_7^{4-}$ peaks divided by 2, areas of PO_4^{3-} peaks, fractions of unreacted $\text{P}_2\text{O}_7^{4-}$ in the residue, X_{DP} , natural logarithms of these fractions, $\ln X_{\text{DP}}$, and first order rate constants, k_1 . The errors reported are probable errors. The fraction of unreacted $\text{P}_2\text{O}_7^{4-}$ was obtained from equation 14:

$$X_{\text{DP}} = (\text{Area } \text{P}_2\text{O}_7^{4-} / 2) / [(\text{Area } \text{P}_2\text{O}_7^{4-} / 2) + \text{Area } \text{PO}_4^{3-}] \quad 14.$$

As the $\text{P}_2\text{O}_7^{4-} + \text{NO}_3^-$ reaction was shown previously by Hubble to be first order with respect to $\text{P}_2\text{O}_7^{4-}$, plots of the natural logarithm of the fraction

Table 3. Summary of residual $P_2O_7^{4-}$ and PO_4^{3-} content at various times at 337° and 342° at a Li^+ concentration of 65.30 cation mol % and first order rate constants for the reaction $Na_4P_2O_7 \rightarrow LiNO_3$.

Reaction time t, min	Area $P_2O_7^{4-}$	$\frac{\text{Area } P_2O_7^{4-}}{2}$	Area PO_4^{3-}	Fraction of total P in residue as $P_2O_7^{4-}$, X_{DP}	$-\ln X_{DP}$
337°					
3.0	33.6	16.8	1.90	0.898	0.10715
6.0	31.8	15.9	2.58	0.860	0.15037
9.0	27.6	13.9	5.20	0.728	0.31780
12.0	26.6	13.3	7.00	0.655	0.42286
15.0	27.3	13.7	6.50	0.678	0.38829
18.0	20.1	10.1	11.7	0.463	0.76938
21.0	24.3	12.2	10.3	0.542	0.61208
$k_1 = (3.31 \pm 0.21) \times 10^{-2} \text{ min}^{-1}$					
342°					
3.0	45.3	22.7	3.80	0.857	0.15478
6.0	28.2	14.1	6.03	0.700	0.35604
9.0	30.5	15.3	9.18	0.625	0.47000
12.0	31.8	15.8	8.75	0.645	0.61619
15.0	27.1	13.6	11.5	0.540	0.63510
18.0	26.6	13.3	11.8	0.530	1.02310
21.0	22.0	11.0	19.6	0.359	
$k_1 = (4.31 \pm 0.21) \times 10^{-2} \text{ min}^{-1}$					

Table 4. Summary of residual $P_2O_7^{4-}$ and PO_4^{3-} content at various times at 347 and 352° at a Li^+ concentration of 65.30 cation mol % and first order rate constants for the reaction $Na_4P_2O_7 - LiNO_3$.

Reaction time t, min	Area $P_2O_7^{4-}$	$\frac{\text{Area } P_2O_7^{4-}}{2}$	Area PO_4^{3-}	Fraction of total P in residue as $P_2O_7^{4-}$, X_{DP}	$-\ln X_{DP}$
347°					
3.0	32.8	16.5	2.00	0.892	0.11441
6.0	26.9	13.5	4.65	0.744	0.29598
9.0	29.8	14.9	8.60	0.634	0.45564
12.2	20.7	10.4	15.2	0.406	0.90079
15.0	19.4	9.68	13.2	0.423	0.86020
18.0	19.0	9.50	20.2	0.320	1.13986
$k_1 = (6.14 \pm 0.24) \times 10^{-2} \text{ min}^{-1}$					
352°					
3.0	36.3	18.1	5.15	0.778	0.25039
6.0	28.6	14.3	9.03	0.613	0.48948
9.0	24.2	12.1	13.5	0.473	0.74939
12.0	18.9	9.45	15.7	0.376	0.97884
15.0	19.8	9.90	17.4	0.363	1.01435
18.0	13.5	6.85	22.3	0.235	1.44821
$k_1 = (7.75 \pm 0.22) \times 10^{-2} \text{ min}^{-1}$					

Table 5. Summary of residual $P_2O_7^{4-}$ and PO_4^{3-} content at various times at 337 and 342° at a Li^+ concentration of 74.31 cation mol % and first order rate constants for the reaction $Na_4P_2O_7 - LiNO_3$.

Reaction time t, min	Area $P_2O_7^{4-}$	$\frac{\text{Area } P_2O_7^{4-}}{2}$	Area PO_4^{3-}	Fraction of total P in residue as $P_2O_7^{4-}$, X_{DP}	$-\ln X_{DP}$
337°					
3.0	33.2	16.6	2.23	0.882	0.12556
6.0	30.1	15.1	4.80	0.759	0.27603
9.0	28.6	14.3	7.20	0.665	0.40780
12.0	27.7	13.9	11.4	0.549	0.59892
15.0	23.6	11.8	14.2	0.454	0.79000
18.0	20.9	10.5	16.0	0.396	0.92577
21.0	18.5	9.25	19.8	0.318	1.14439
$k_1 = (5.19 \pm 0.05) \times 10^{-2} \text{ min}^{-1}$					
342°					
3.0	31.1	15.6	2.80	0.848	0.16508
6.1	32.4	16.2	6.70	0.707	0.34613
9.0	23.3	11.7	9.60	0.549	0.59912
12.1	23.7	11.9	12.5	0.488	0.71805
15.0	22.9	11.5	16.7	0.408	0.89698
18.0	17.7	8.85	19.3	0.314	1.15713
21.0	17.5	8.76	20.7	0.297	1.21284
$k_1 = (6.05 \pm 0.10) \times 10^{-2} \text{ min}^{-1}$					

Table 6. Summary of residual $P_2O_7^{4-}$ and PO_4^{3-} content at various times at 347 and 352° at a Li^+ concentration of 74.31 cation mol % and first order rate constants for the reaction $Na_4P_2O_7 - LiNO_3$.

Reaction time t, min	Area $P_2O_7^{4-}$	$\frac{\text{Area } P_2O_7^{4-}}{2}$	Area PO_4^{3-}	Fraction of total P in residue as $P_2O_7^{4-}$, X_{DP}	$-\ln X_{DP}$
347°					
3.0	38.8	19.4	4.20	0.822	0.19597
6.0	30.4	15.2	10.0	0.603	0.50555
9.0	27.1	13.6	10.4	0.567	0.56798
12.0	20.5	10.3	16.4	0.386	0.95252
15.0	19.1	9.55	20.7	0.316	1.15296
18.0	18.6	9.30	26.5	0.260	1.34793
$k_1 = (7.54 \pm 0.17) \times 10^{-2} \text{ min}^{-1}$					
352°					
3.0	32.9	16.5	4.90	0.771	0.26003
6.0	26.0	13.0	9.40	0.580	0.54411
9.0	26.0	13.0	15.8	0.451	0.79543
12.0	17.3	8.65	20.3	0.299	1.20801
15.1	18.3	9.15	24.8	0.270	1.31113
18.0	11.8	5.90	27.2	0.178	1.72458
$k_1 = (9.31 \pm 0.18) \times 10^{-2} \text{ min}^{-1}$					

Table 7. Summary of residual $P_2O_7^{4-}$ and PO_4^{3-} content at various times at 337 and 342° at a Li^+ concentration of 83.77 cation mol % and first order rate constants for the reaction $Na_4P_2O_7 - LiNO_3$.

Reaction time t, min	Area $P_2O_7^{4-}$	$\frac{\text{Area } P_2O_7^{4-}}{2}$	Area PO_4^{3-}	Fraction of total P in residue as $P_2O_7^{4-}$, X_{DP}	$-\ln X_{DP}$
337°					
3.0	38.7	19.4	2.50	0.886	0.12121
6.0	41.6	20.8	6.93	0.750	0.28756
9.0	24.6	12.3	9.50	0.564	0.57231
12.0	21.3	10.7	11.3	0.486	0.72080
15.0	19.1	9.56	13.9	0.408	0.89771
18.0	19.1	9.56	17.9	0.348	1.05583
$k_1 = (5.90 \pm 0.10) \times 10^{-2} \text{ min}^{-1}$					
342°					
3.0	36.2	18.1	4.00	0.819	0.19967
6.0	30.7	15.4	9.70	0.614	0.48850
9.0	22.2	11.1	9.28	0.545	0.60761
12.0	19.4	9.70	12.2	0.443	0.81436
15.8	21.2	10.6	18.3	0.367	1.00299
$k_1 = (7.23 \pm 0.29) \times 10^{-2} \text{ min}^{-1}$					

Table 8. Summary of residual $P_2O_7^{4-}$ and PO_4^{3-} content at various times at 347 and 352° at a Li^+ concentration of 83.77 cation mol % and first order rate constants for the reaction $Na_4P_2O_7 \rightarrow LiNO_3$.

Reaction time t, min	Area $P_2O_7^{4-}$	$\frac{\text{Area } P_2O_7^{4-}}{2}$	Area PO_4^{3-}	Fraction of total P in residue as $P_2O_7^{4-}$, X_{DP}	$-\ln X_{DP}$
347°					
3.0	31.6	15.9	4.70	0.772	0.25877
6.0	26.1	13.1	12.0	0.522	0.65026
9.0	21.9	11.0	15.7	0.412	0.88677
12.0	15.1	7.55	16.3	0.317	1.15024
15.0	13.1	6.55	22.5	0.225	1.48955
18.2	12.5	6.25	27.8	0.184	1.69525
$k_1 = (9.64 \pm 0.13) \times 10^{-2} \text{ min}^{-1}$					
352°					
3.0	29.7	14.9	4.38	0.773	0.25771
4.0	24.4	12.2	5.58	0.686	0.37664
6.0	21.2	10.6	15.8	0.402	0.91251
9.0	17.1	8.55	20.7	0.292	1.22995
12.0	7.50	3.75	11.2	0.251	1.38296
14.0	8.78	4.39	21.2	0.172	1.76026
$k_1 = (12.46 \pm 0.46) \times 10^{-2} \text{ min}^{-1}$					

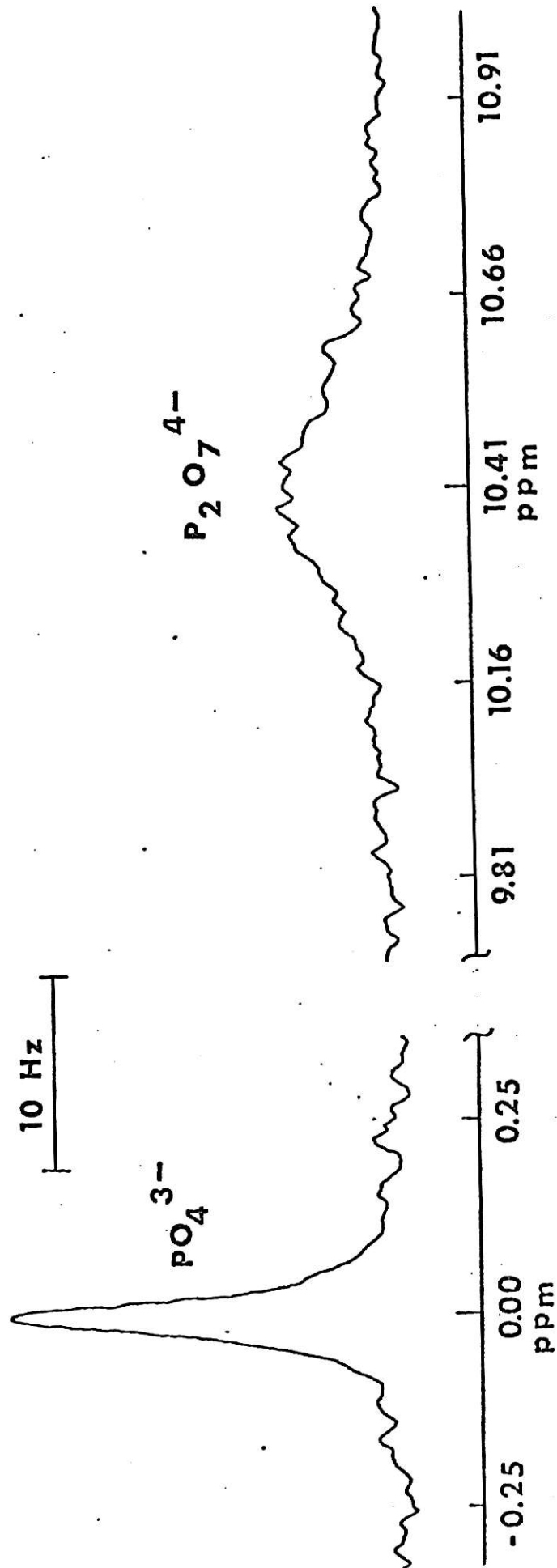


Fig. 6. Time average ^{31}P nmr spectrum of an aqueous⁺ sample obtained from the $\text{Na}_4\text{P}_2\text{O}_7^{4-}$ LiNO_3 reaction at 342° quenched after 15 min at a Li^+ concentration of 74.31 cation mol %.

of unreacted $P_2O_7^{4-}$, $\ln X_{DP}$, versus reaction time, t (min), gave reasonably straight lines. These lines yielded the rate constants, k_1 , at various temperatures and cation mole percents of Li^+ . The rate constants came from least squares slopes of the lines forced through the origin (28). Application of the statistical F test (28), using 5% critical values for F , confirmed that in all but one case no sufficient evidence was present to warrant the assertion that an intercept differed from the origin more than could be accounted for by experimental errors. The exception was the run made at 337° and a Li^+ cation mole percent of 74.31%. This one case cannot be explained other than by commenting that the difference of F values was not extremely large. Additional points were unable to improve the fit.

Figures 7 through 12 show the plots of the natural logarithm of the fraction of unreacted $P_2O_7^{4-}$, $\ln X_{DP}$, versus reaction time, t (min). Figures 7, 8, 11, and 12 show the greatest amount of scatter, while Figures 9 and 10 show the least scatter. This can be explained by the change in temperature and mole percent of Li^+ cation. At high temperatures and large concentrations of Li^+ the scatter was due to more rapid reaction, which gave rise to larger experimental errors in interval times. Figures 11 and 12 show scatter of this nature. At low temperatures and small concentrations of Li^+ the observed scatter was probably due to precipitation in the reacting melt of some material of unknown composition during the course of reaction. Figures 7 and 8 illustrate scatter apparently caused by the formation of a slight quantity of this insoluble material. This material increased in abundance as the temperature and/or Li^+ concentration were further reduced. Thus, it was found that a 50 cation mole percent of Li^+ solvent was totally unsuitable for a kinetics study of the reaction. It was observed that upon addition of $Na_4P_2O_7$, a slight reaction would occur and a large amount of precipitate would appear. A first order plot of the data gave such an extremely large amount of scatter that it was impossible to get an acceptable rate constant. Thus, a 65.30 cation mole percent Li^+ concentration was the lowest limit of study for the reaction. Below this concentration of Li^+ the scatter becomes too great.

The normal Arrhenius plots of $\ln k_1$ versus $1/T$ ($^\circ K$) $^{-1}$, based on

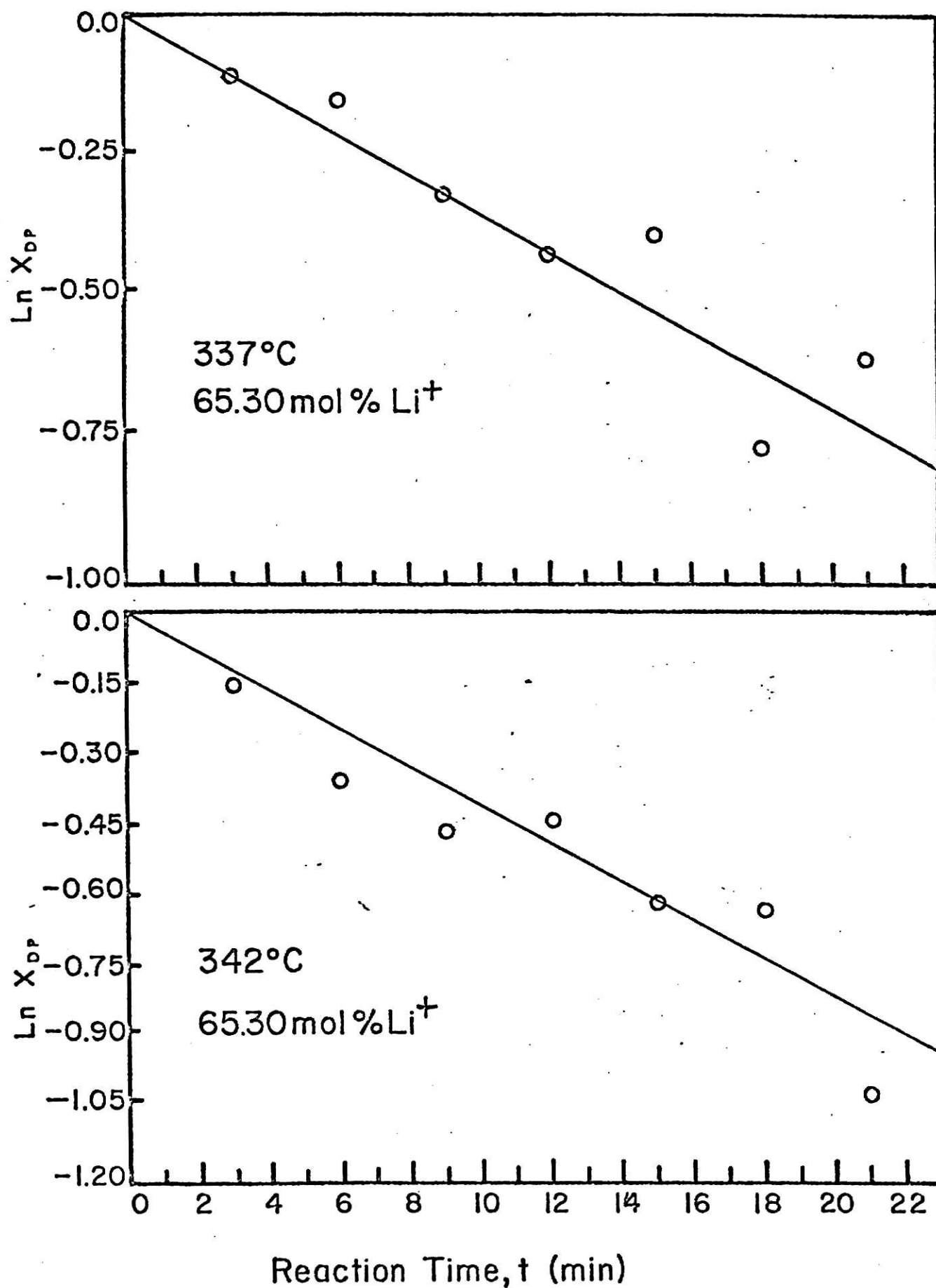
$$k_1 = A \exp(-E_a/RT) \quad 17.$$

are in Fig. 13. The more complete transition state plots of $\ln (k_1/T)$ versus

Explanation of Plate II.

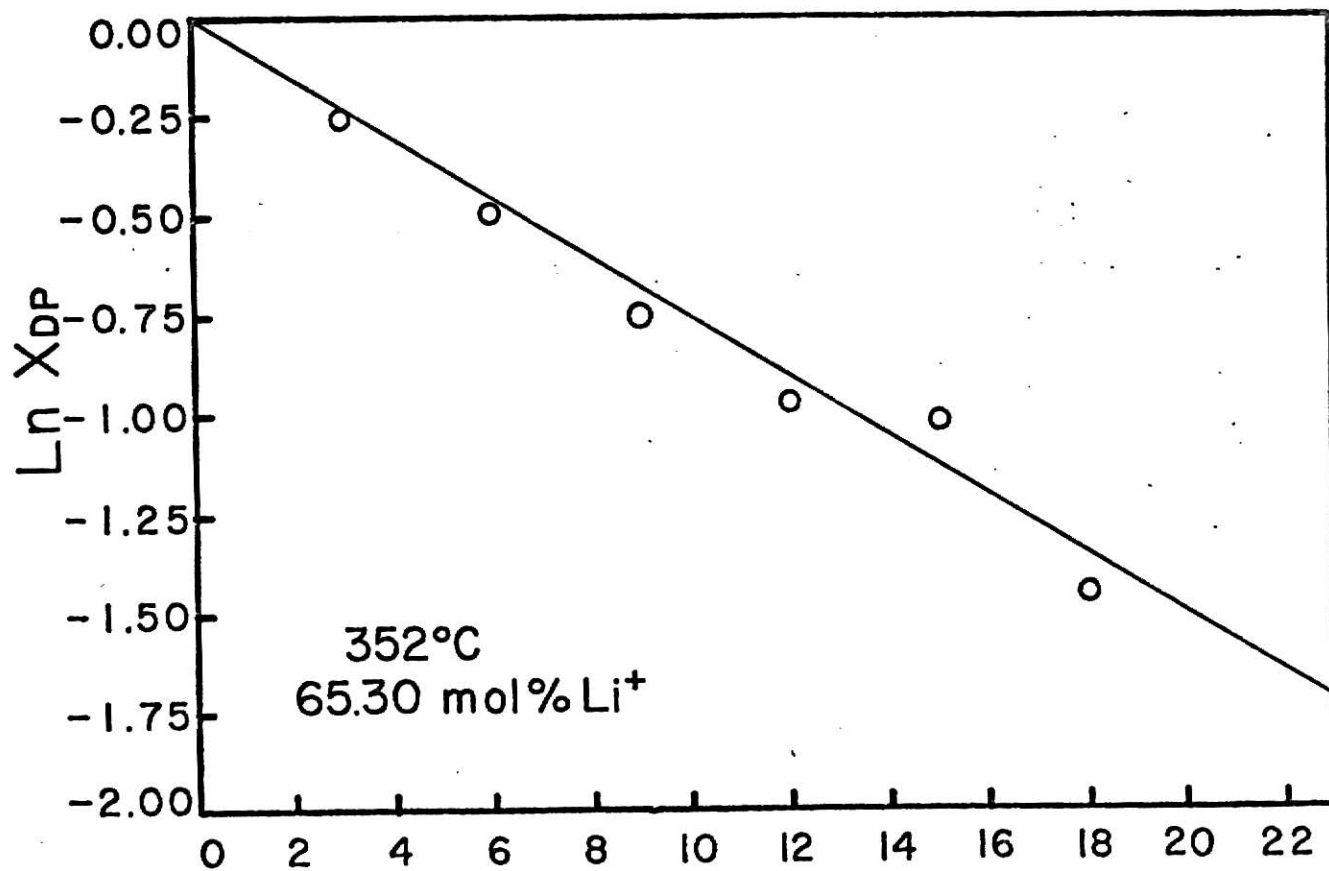
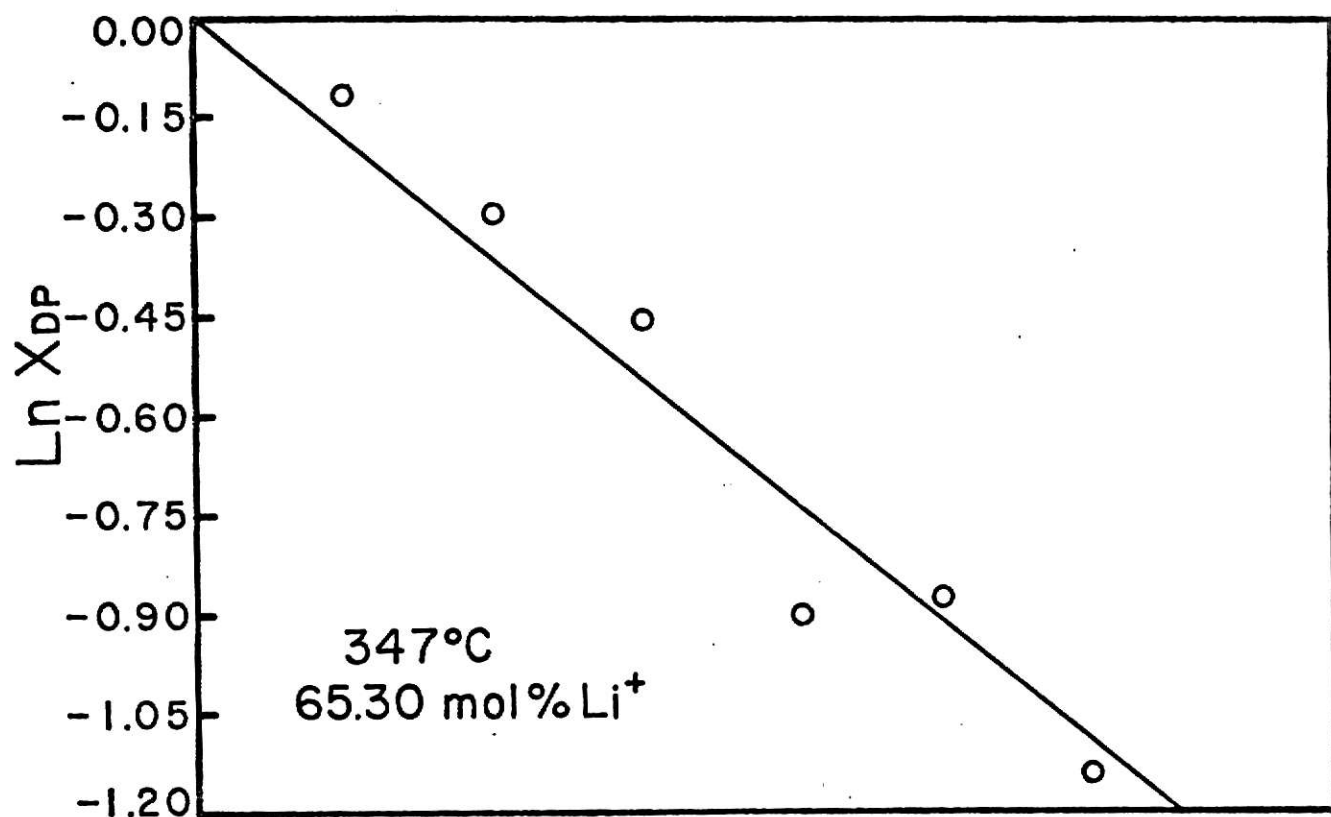
Fig. 7. Plots of the natural logarithm of the fraction of unreacted diphosphate anion, $\ln X_{DP}$, versus reaction time, t (min), at 337 and 342° at a concentration of Li^+ of 65.30 cation mol %.

Plate II



Explanation of Plate III.

Fig. 8. Plots of the natural logarithm of the fraction of unreacted diphosphate anion, $\ln X_{DP}$, versus reaction time, t (min), at 347 and 352° at a concentration of Li^+ of 65.30 cation mol %.



Reaction Time, t (min)

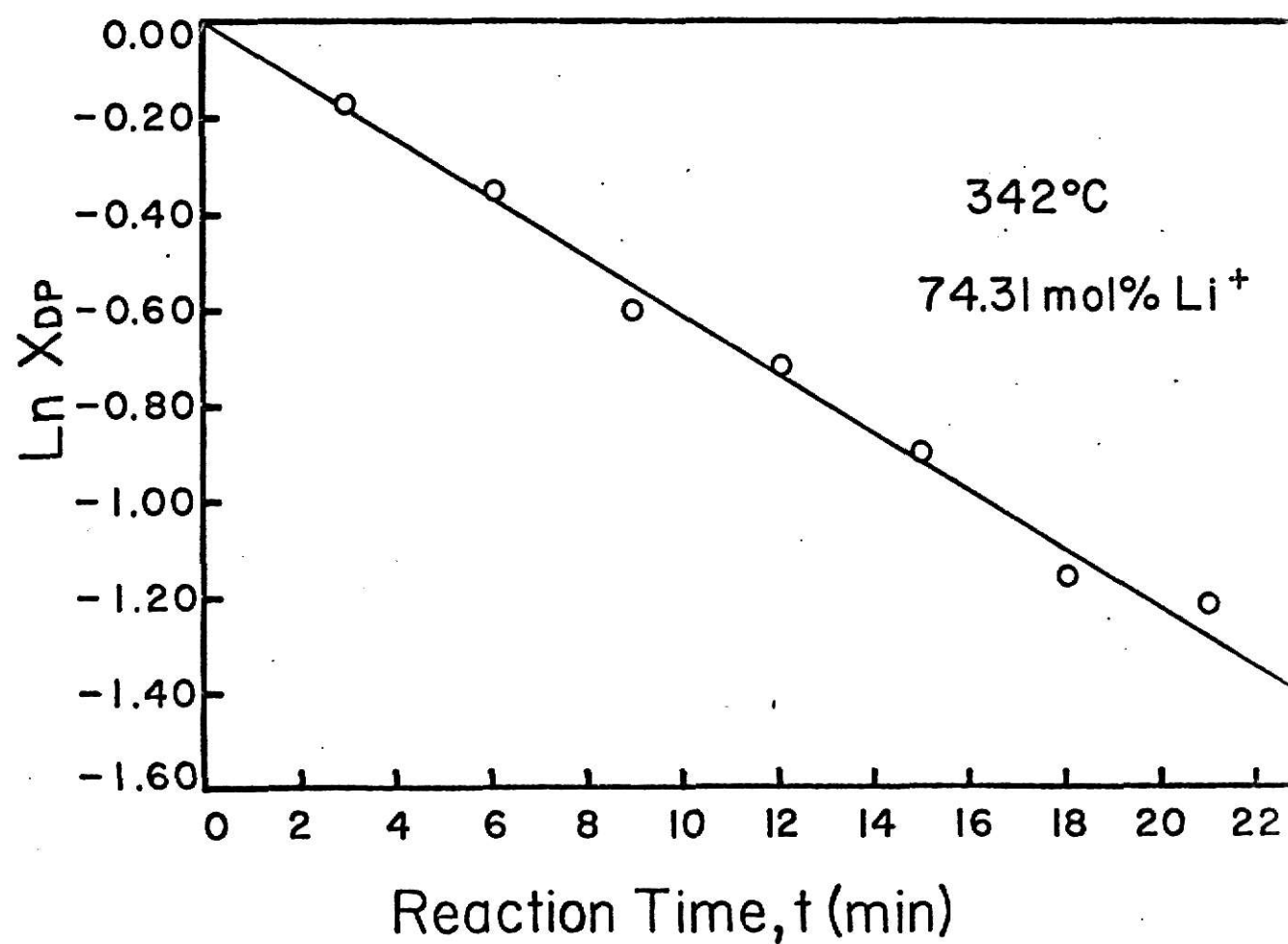
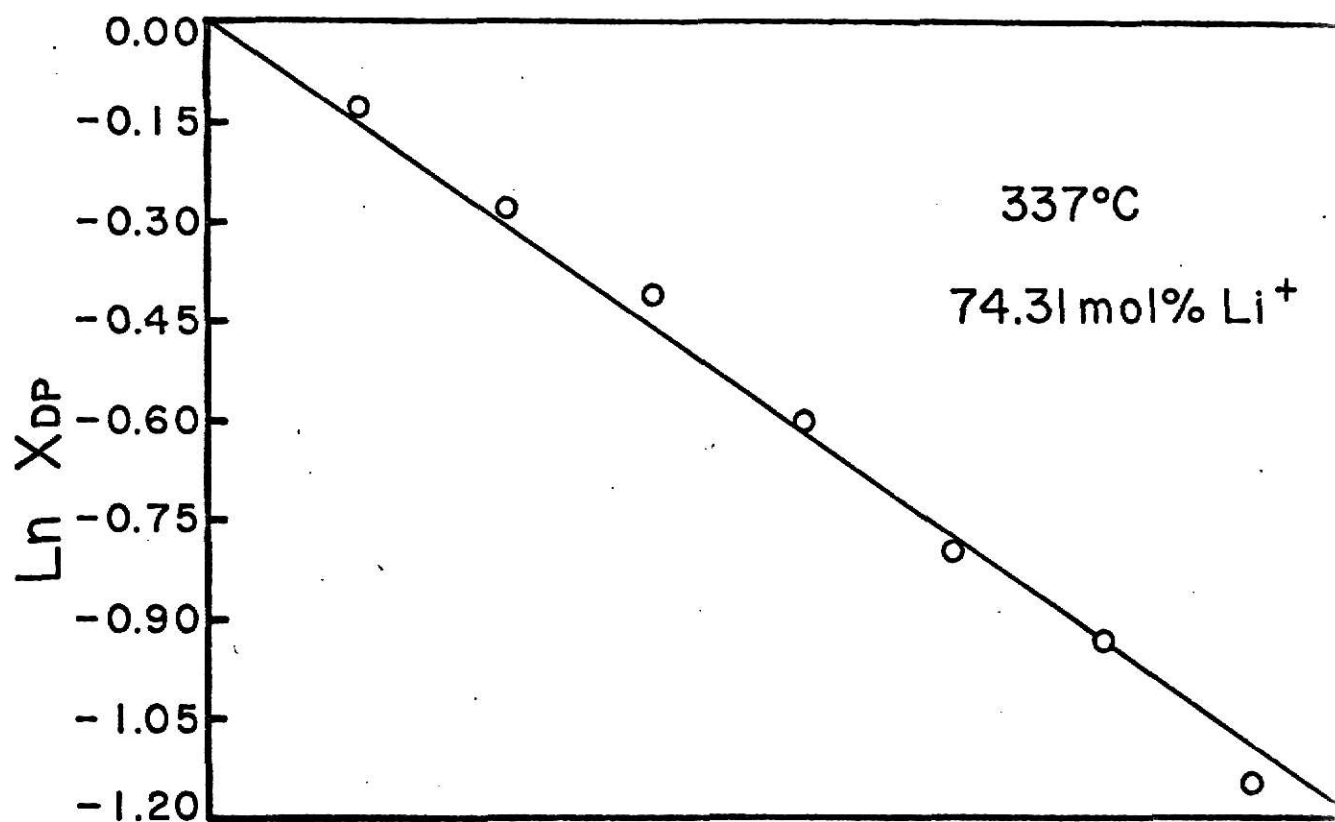
Explanation of Plate IV.

Fig. 9. Plots of the natural logarithm of the fraction of unreacted diphosphate anion, $\ln X_{DP}$, versus reaction time, t (min), at 337 and 342° at a concentration of Li^+ of 74.31 cation mol %.

**THIS BOOK
CONTAINS
NUMEROUS
PAGES THAT ARE
CUT OFF**

**THIS IS AS
RECEIVED FROM
THE CUSTOMER**

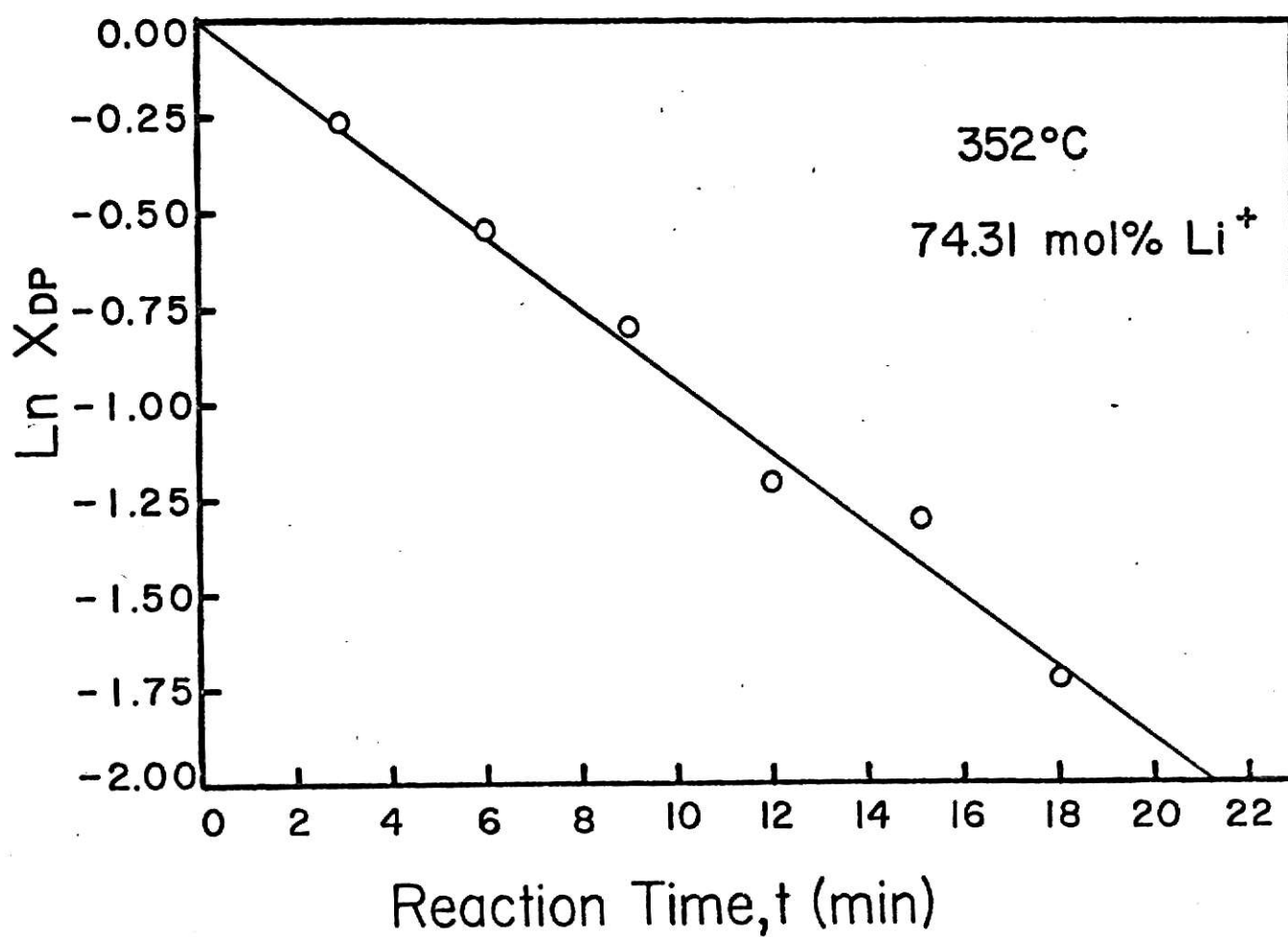
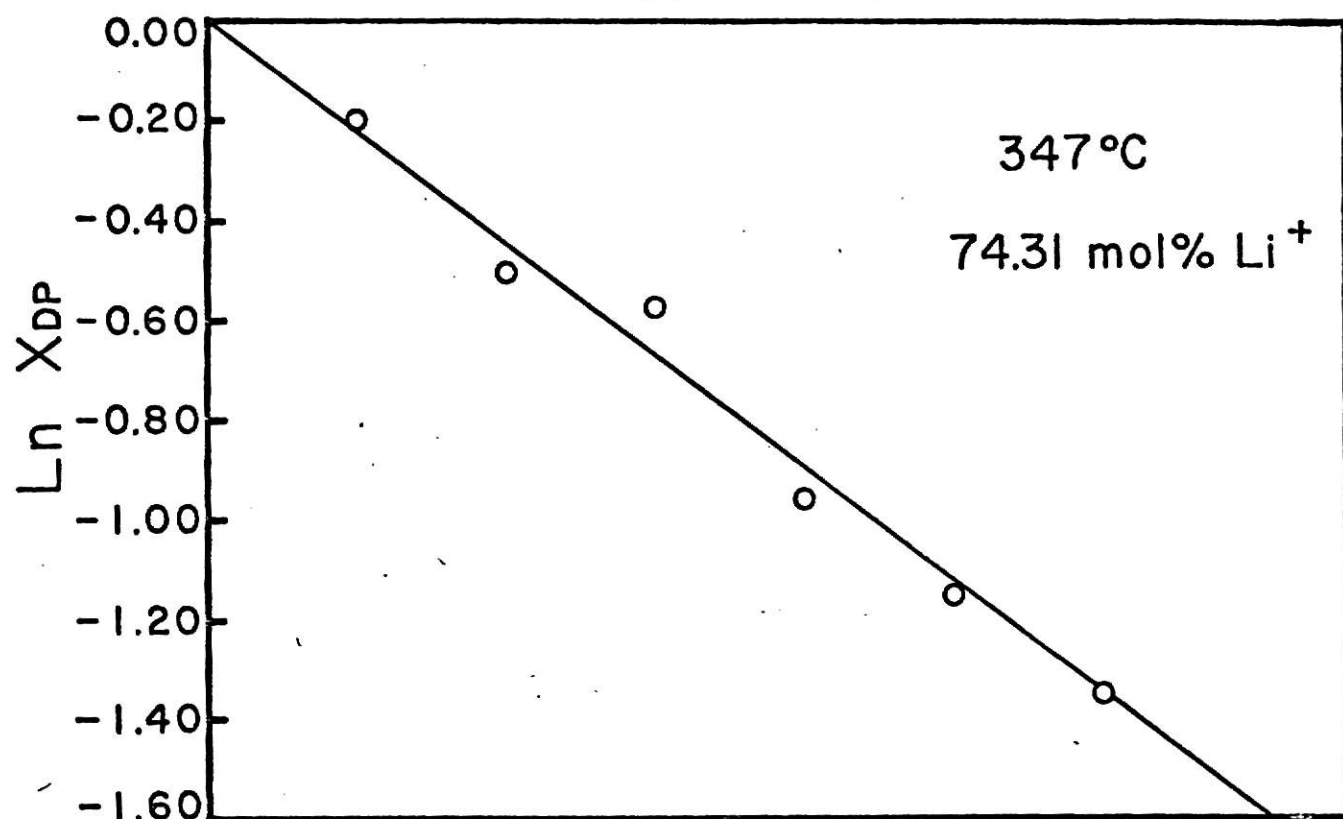
Plate IV



Explanation of Plate V.

Fig. 10. Plots of the natural logarithm of the fraction of unreacted diphosphate anion, $\ln X_{DP}$, versus reaction time, t (min), at 347 and 352° at a concentration of Li^+ of 74.31 cation mol %.

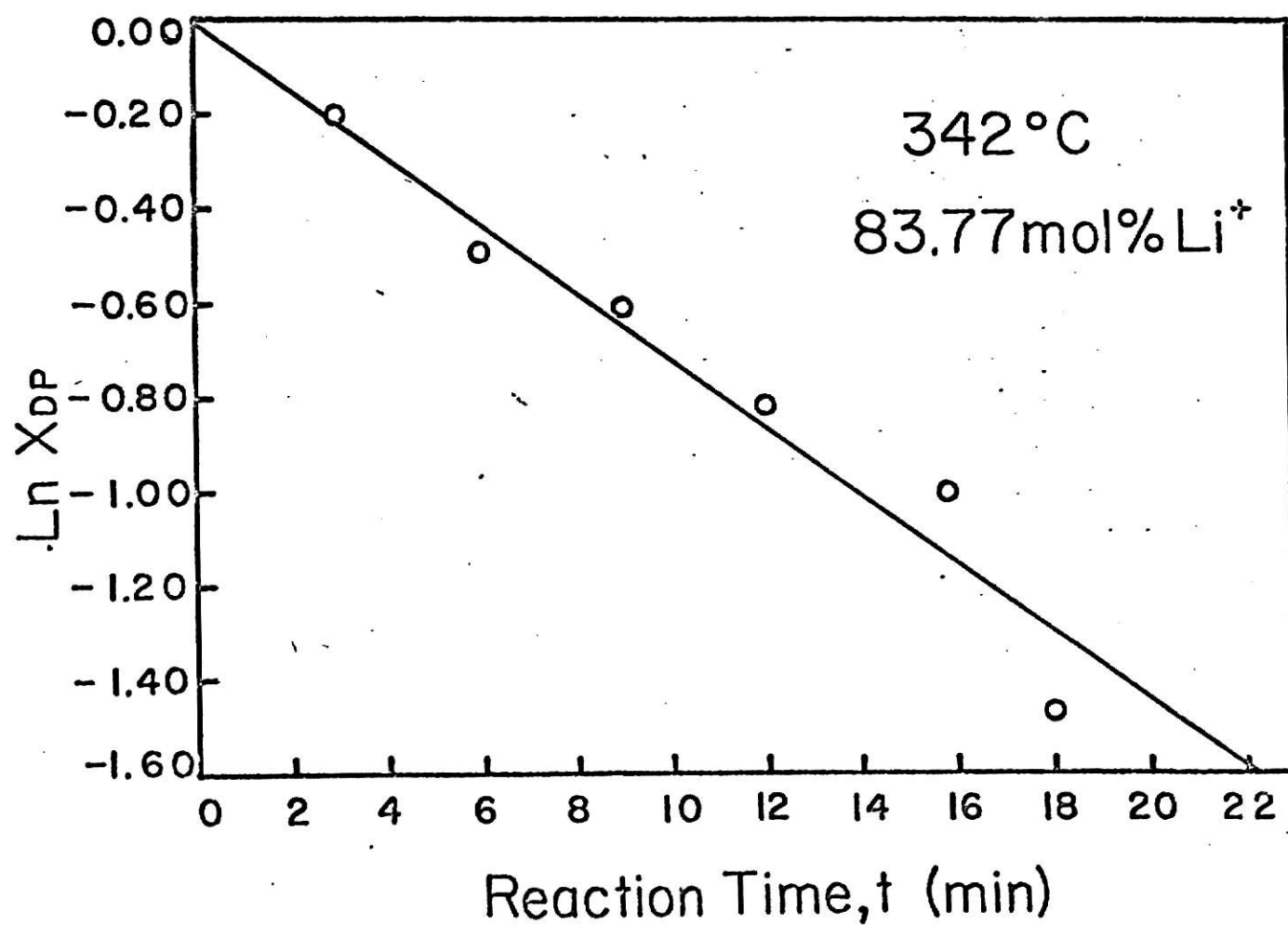
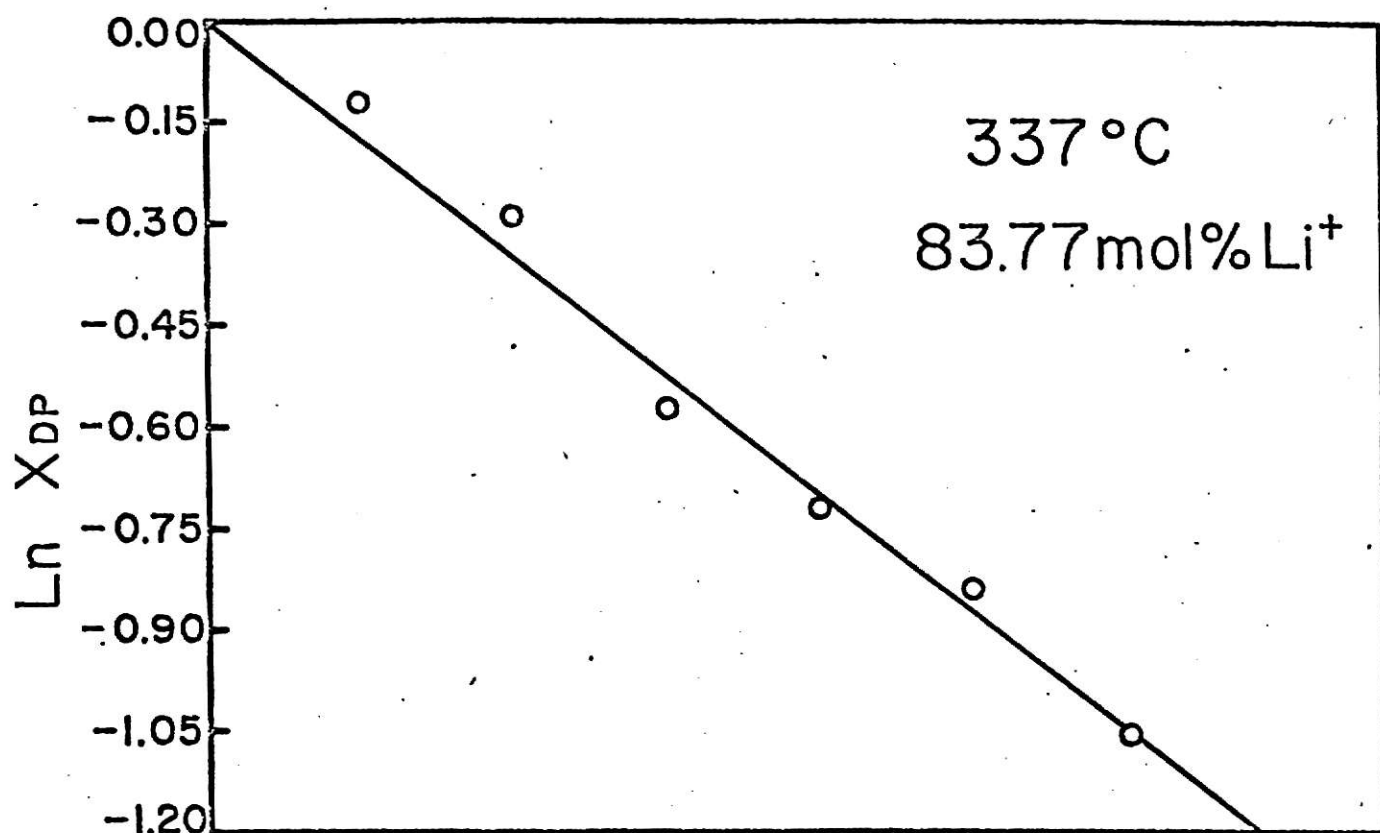
Plate V



Explanation of Plate VI.

Fig. 11. Plots of the natural logarithm of the fraction of unreacted diphosphate anion, $\ln X_{\text{DP}}$, versus reaction time, t (min), at 337 and 342° at a concentration of Li^+ of 83.77 cation mol %.

Plate VI

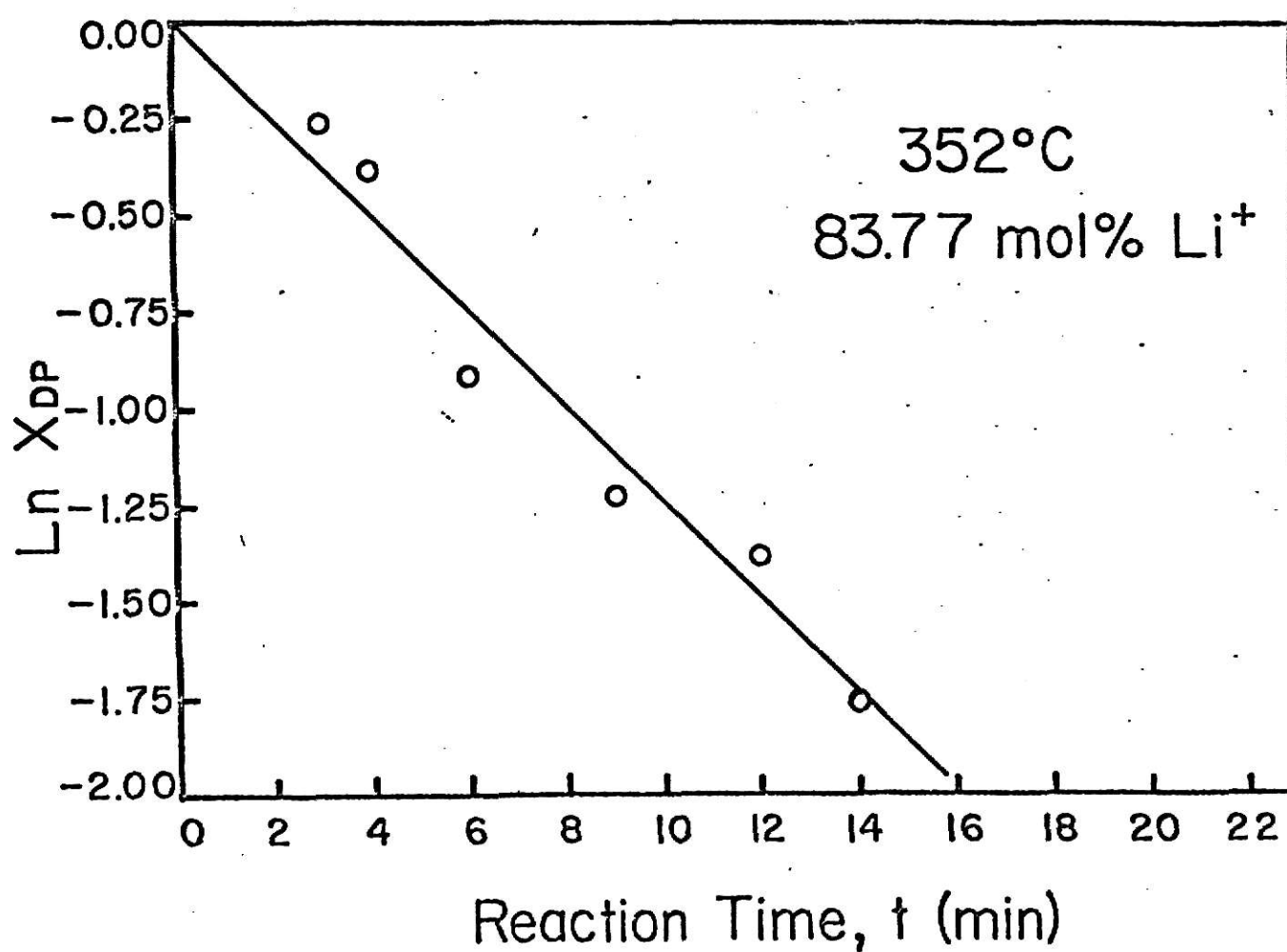
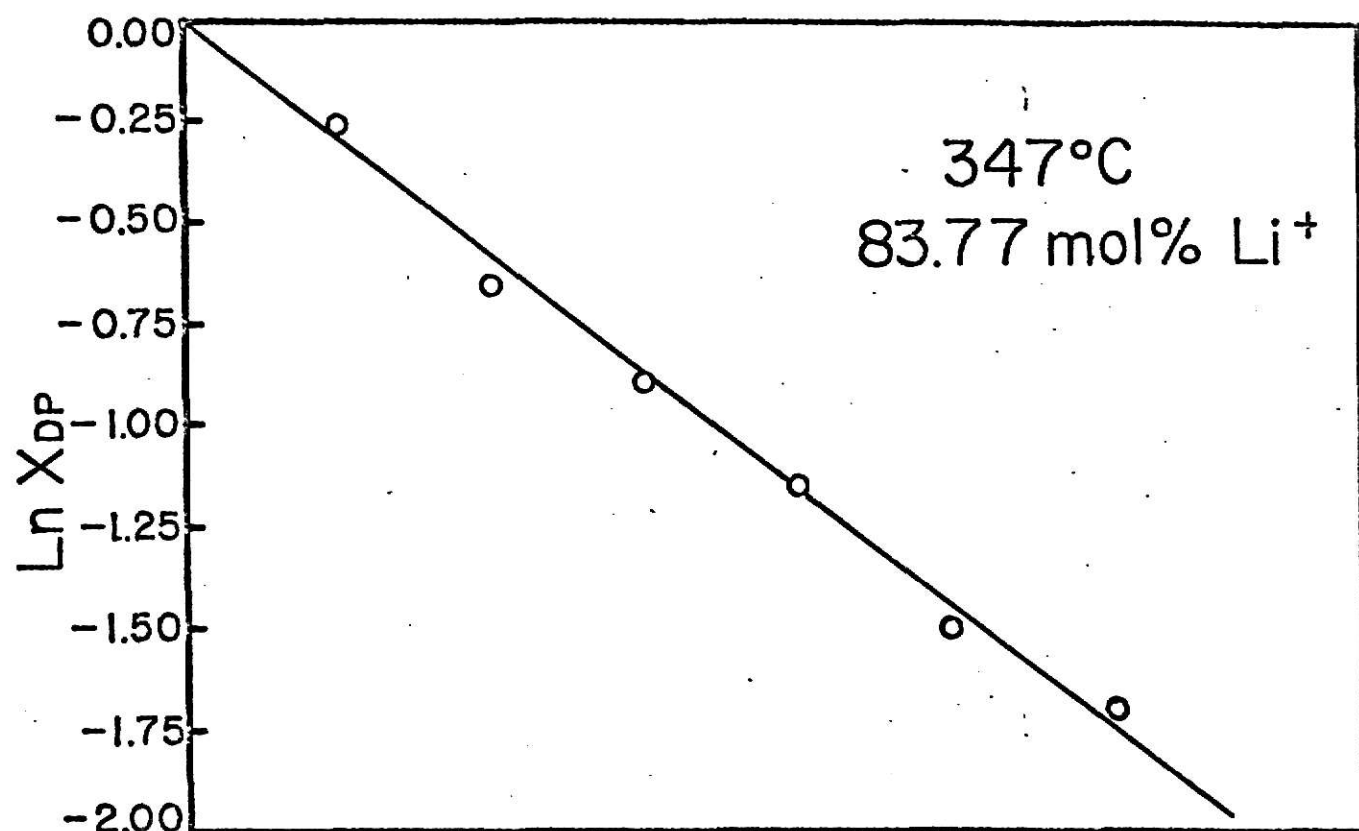


Explanation of Plate Vii.

Fig. 12. Plots of the natural logarithm of the fraction of unreacted diphosphate anion, $\ln X_{DP}$, versus reaction time, t (min), at 347 and 352° at a concentration of Li^+ of 83.77 cation mol %.

Plate

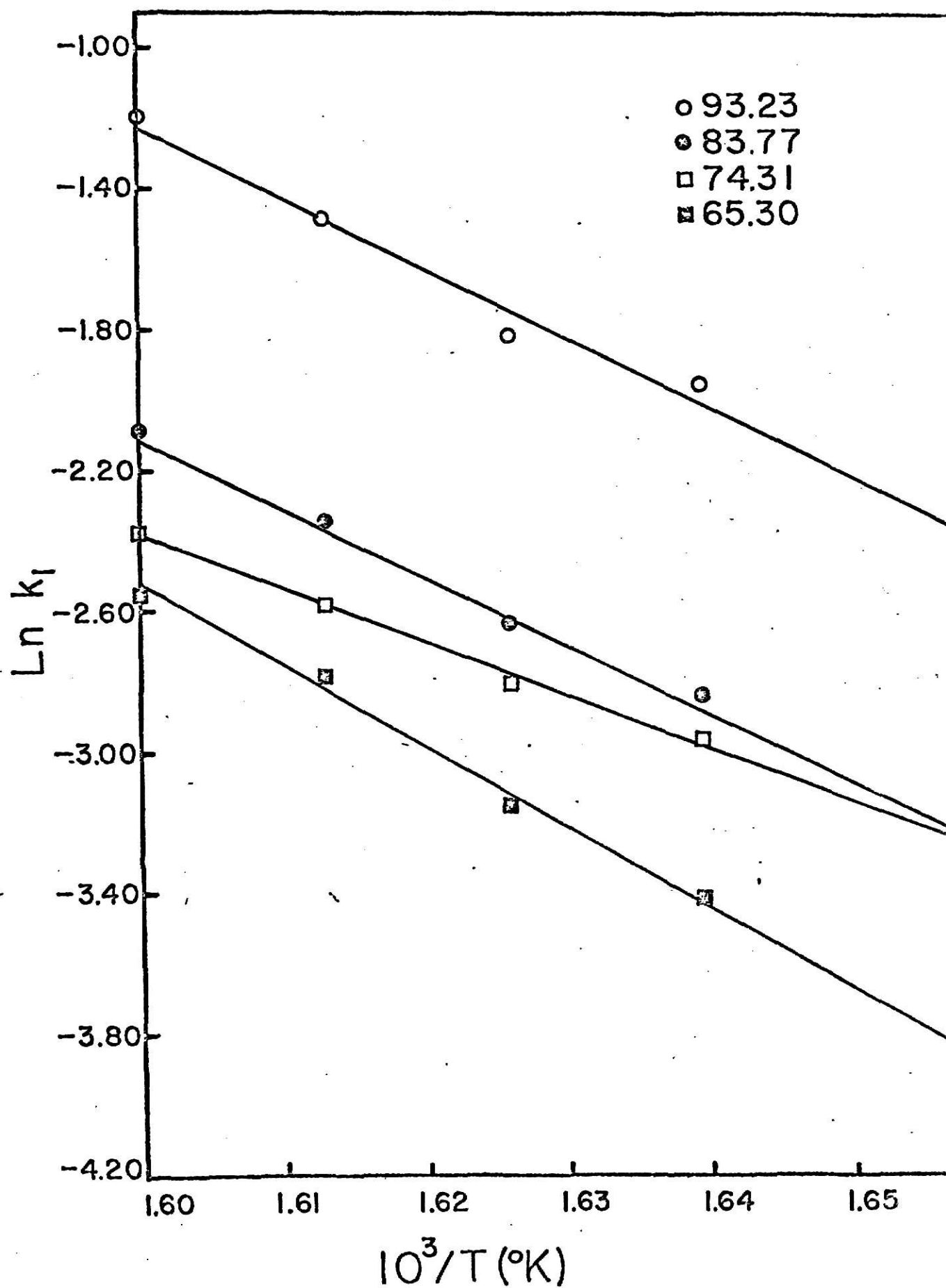
VII



Explanation of Plate VIII.

Fig. 13. Plots of the natural logarithm of the first order rate constants, $\ln k_1$, versus $1/T$ ($^{\circ}\text{K}$) $^{-1}$ for the $\text{Na}_4\text{P}_2\text{O}_7 - \text{LiNO}_3$ reaction at 65.30, 74.31, 83.77, and 93.23 cation mol %.

Plate VIII



$(1/T) (^{\circ}\text{K})^{-1}$, in Fig. 14, are based on the equation:

$$k_1 = (ekT/h) \exp(\Delta S^{\ddagger}/R) \exp(-E_a/RT) \quad 23.$$

The least squares slopes of the straight lines of Fig. 13 yield the activation energies and the least squares intercepts yield the activation entropies calculated at a temperature of 600°K from:

$$\ln A = \ln (ekT/h) + \Delta S^{\ddagger}/R \quad 18.$$

The least squares slopes of the straight lines of Figure 14 yield the activation energies, and the least squares intercepts yield the activation entropies, again calculated at a temperature of 600°K from:

$$\ln A' = \ln (ek/h) + \Delta S^{\ddagger}/R \quad 24.$$

All of the above values are listed in Table 9, with equations for the straight lines of Figures 13 and 14 at the various concentrations of Li^+ . The results calculated from Arrhenius and $\ln (k_1/T)$ versus $1/T$ plots for the 74.31 cation mol % data are not reliable. This is the result of what could be poor data as far as temperature dependence is concerned. The last point at 337° of both plots, if omitted, would give the lines about the same slopes as for the other concentrations, thus making the E_a about the same as the others. Thus, the activation energy and entropy results of the 74.31 Li^+ cation mol % should not be highly regarded. The errors reported in Table 9 are probable errors.

Figures 15 through 17 contain plots of the natural logarithm of the fraction of unreacted $\text{P}_2\text{O}_7^{4-}$, $\ln X_{\text{DP}}$, versus reaction time, t (min). These are arranged for comparison of the effects of temperature. Figure 15 contains plots of the runs made at the 65.30 cation mol % Li^+ concentration at 337, 342, 347, and 352°. Figures 16 and 17 contain similar plots of the runs made at the 74.31 and 83.77 cation mol % Li^+ concentrations, respectively. These three figures show basically the same effects of temperature at any of the three concentrations of Li^+ .

Figures 18 through 21 illustrate further comparisons of the data. In these figures the effects of changing the concentration are examined at given temperatures. Thus, Figure 18 is a comparison of the different cation mol %'s of Li^+ . This figure and subsequent figures contain the results of the 93.23

Explanation of Plate IX.

Fig. 14. Plots of the natural logarithm of k_1/T ($\text{min } ^\circ\text{K}^{-1}$), $\ln (k_1/T)$, versus $1/T$ ($^\circ\text{K}^{-1}$) for the reaction $\text{Na}_4\text{P}_2\text{O}_7 - \text{LiNO}_3$ at 65.30, 74.31, 83.77, and 93.23 cation mol %.

Plate IX

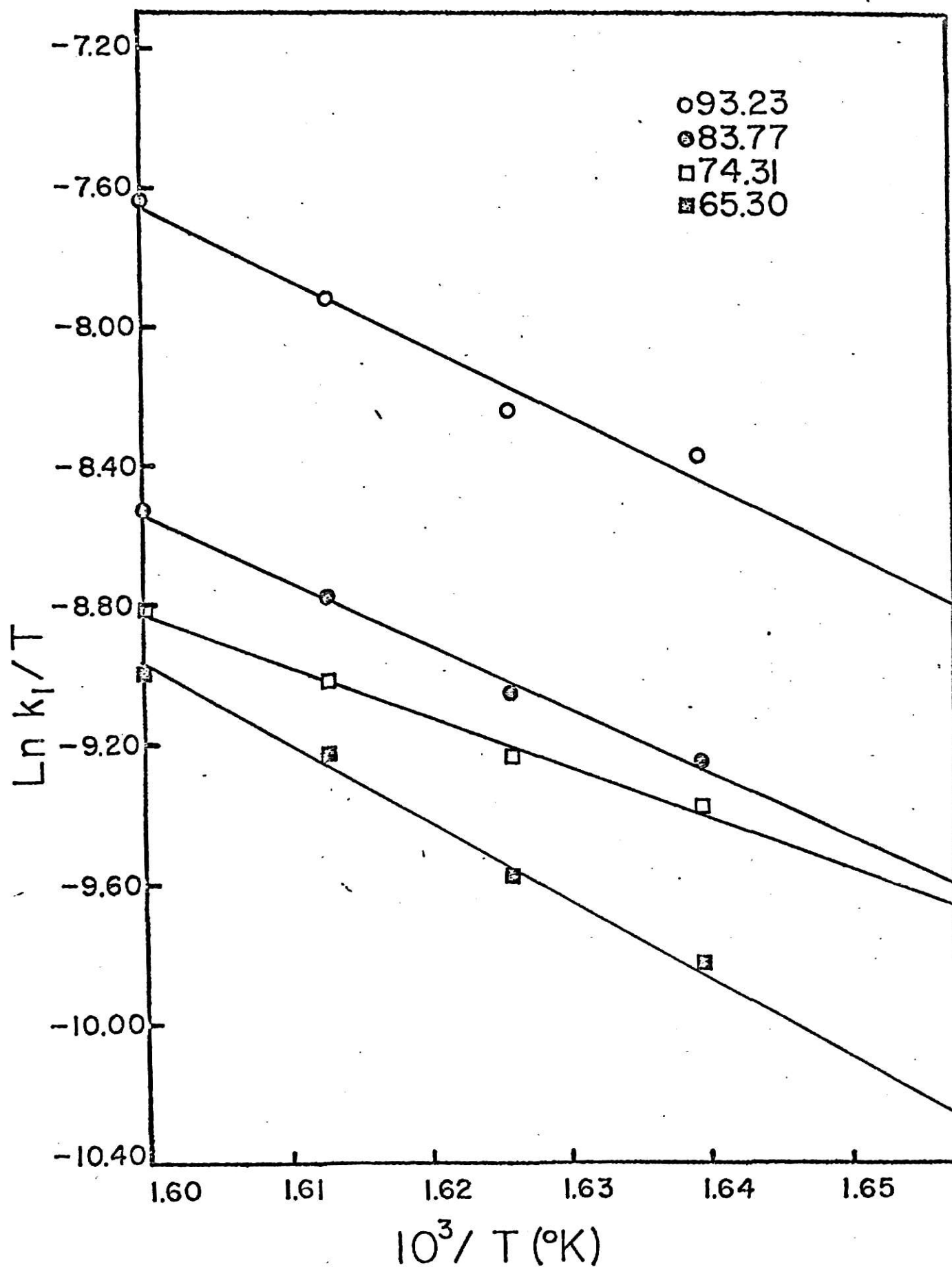


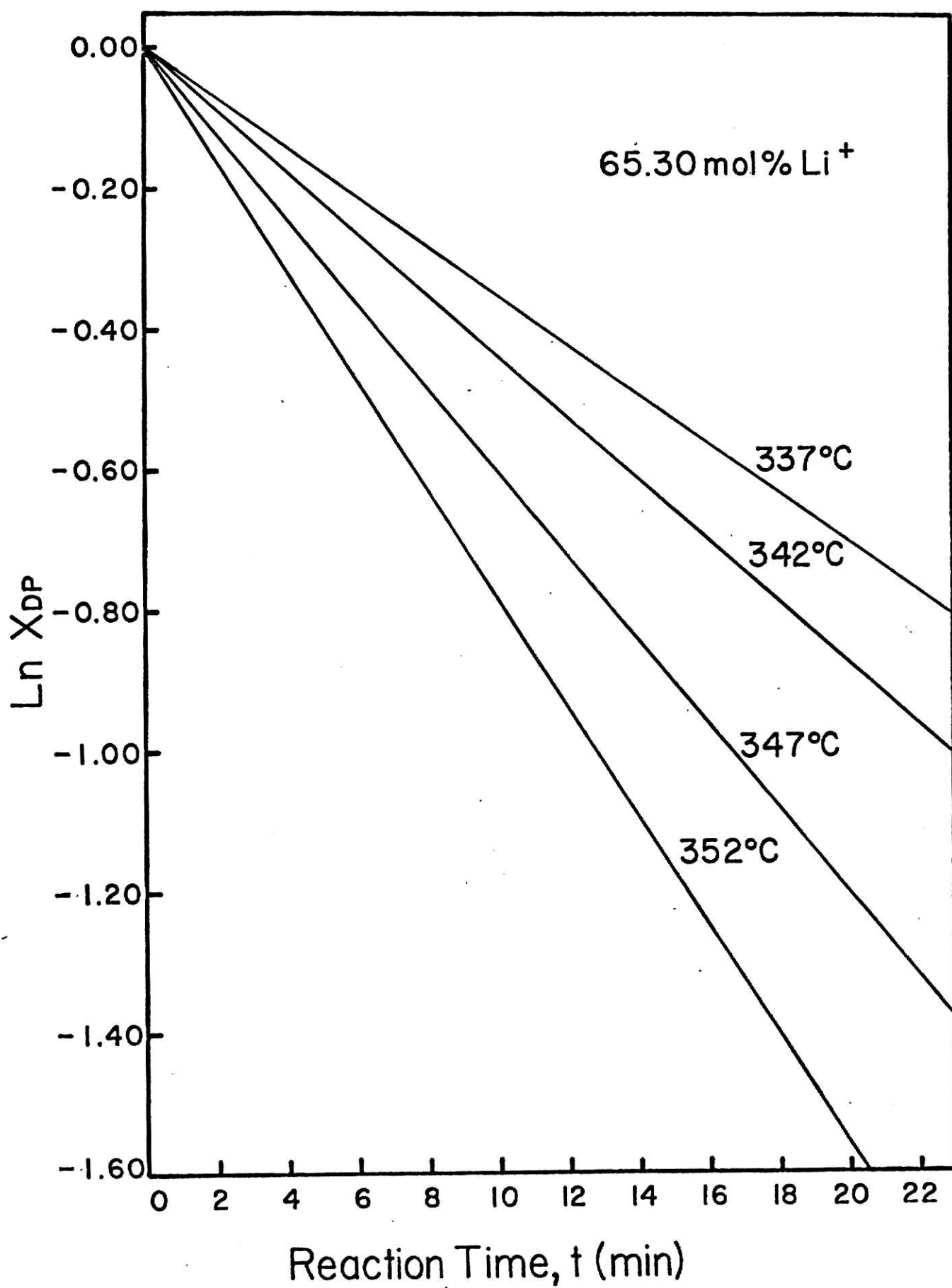
Table 9. Summary of preexponential factors, activation energies, and entropies calculated from an Arrhenius plot and from a plot of $\ln (k_1/T)$ versus $(1/T)$ ($^{\circ}\text{K}^{-1}$) and least squares equations for best straight lines from both plots at various Li^+ concentrations.

Li^+ conc., mol % Li^+	Preexponential factors, A, min^{-1}	$\ln k_1$ versus $1/T$		E_a kcal mol^{-1}	ΔS^\ddagger e.u. mol^{-1}
		$\ln k_1$ (k_1 in min^{-1})	$\ln k_1$ (k_1 in min^{-1})		
65.30	1.98×10^{14}	$(32.92 \pm 1.54) - (2.22 \pm 0.10) \times 10^4(1/T)$	$(32.92 \pm 1.54) - (2.22 \pm 0.10) \times 10^4(1/T)$	44.04 ± 1.89	-4.63 ± 3.06
74.31	2.60×10^9	$(21.68 \pm 1.15) - (1.50 \pm 0.07) \times 10^4(1/T)$	$(21.68 \pm 1.15) - (1.50 \pm 0.07) \times 10^4(1/T)$	29.89 ± 1.41	-26.98 ± 2.29
83.77	3.12×10^{12}	$(28.77 \pm 1.28) - (1.93 \pm 0.08) \times 10^4(1/T)$	$(28.77 \pm 1.28) - (1.93 \pm 0.08) \times 10^4(1/T)$	38.33 ± 1.57	-12.88 ± 2.54
93.23	1.52×10^{13}	$(30.35 \pm 3.11) - (1.97 \pm 0.19) \times 10^4(1/T)$	$(30.35 \pm 3.11) - (1.97 \pm 0.19) \times 10^4(1/T)$	39.21 ± 5.66	-9.75 ± 9.16

Li^+ conc., mol % Li^+	Preexponential factors, A, min^{-1}	$\ln (k_1/T)$ versus $1/T$		E_a' kcal mol^{-1}	$\Delta S^\ddagger'$ e.u. mol^{-1}
		$\ln (k_1/T)$ (k_1 in min^{-1})	$\ln (k_1/T)$ (k_1 in min^{-1})		
65.30	1.18×10^{11}	$(25.49 \pm 1.54) - (2.15 \pm 0.10) \times 10^4(1/T)$	$(25.49 \pm 1.54) - (2.15 \pm 0.10) \times 10^4(1/T)$	42.82 ± 1.89	-6.68 ± 3.06
74.31	1.54×10^6	$(14.25 \pm 1.15) - (1.44 \pm 0.07) \times 10^4(1/T)$	$(14.25 \pm 1.15) - (1.44 \pm 0.07) \times 10^4(1/T)$	28.66 ± 1.41	-29.02 ± 2.29
83.77	1.85×10^9	$(21.34 \pm 1.28) - (1.87 \pm 0.08) \times 10^4(1/T)$	$(21.34 \pm 1.28) - (1.87 \pm 0.08) \times 10^4(1/T)$	37.10 ± 1.56	-14.93 ± 2.53
93.23	9.00×10^9	$(22.92 \pm 3.10) - (1.91 \pm 0.19) \times 10^4(1/T)$	$(22.92 \pm 3.10) - (1.91 \pm 0.19) \times 10^4(1/T)$	37.99 ± 3.81	-11.79 ± 6.17

Explanation of Plate X.

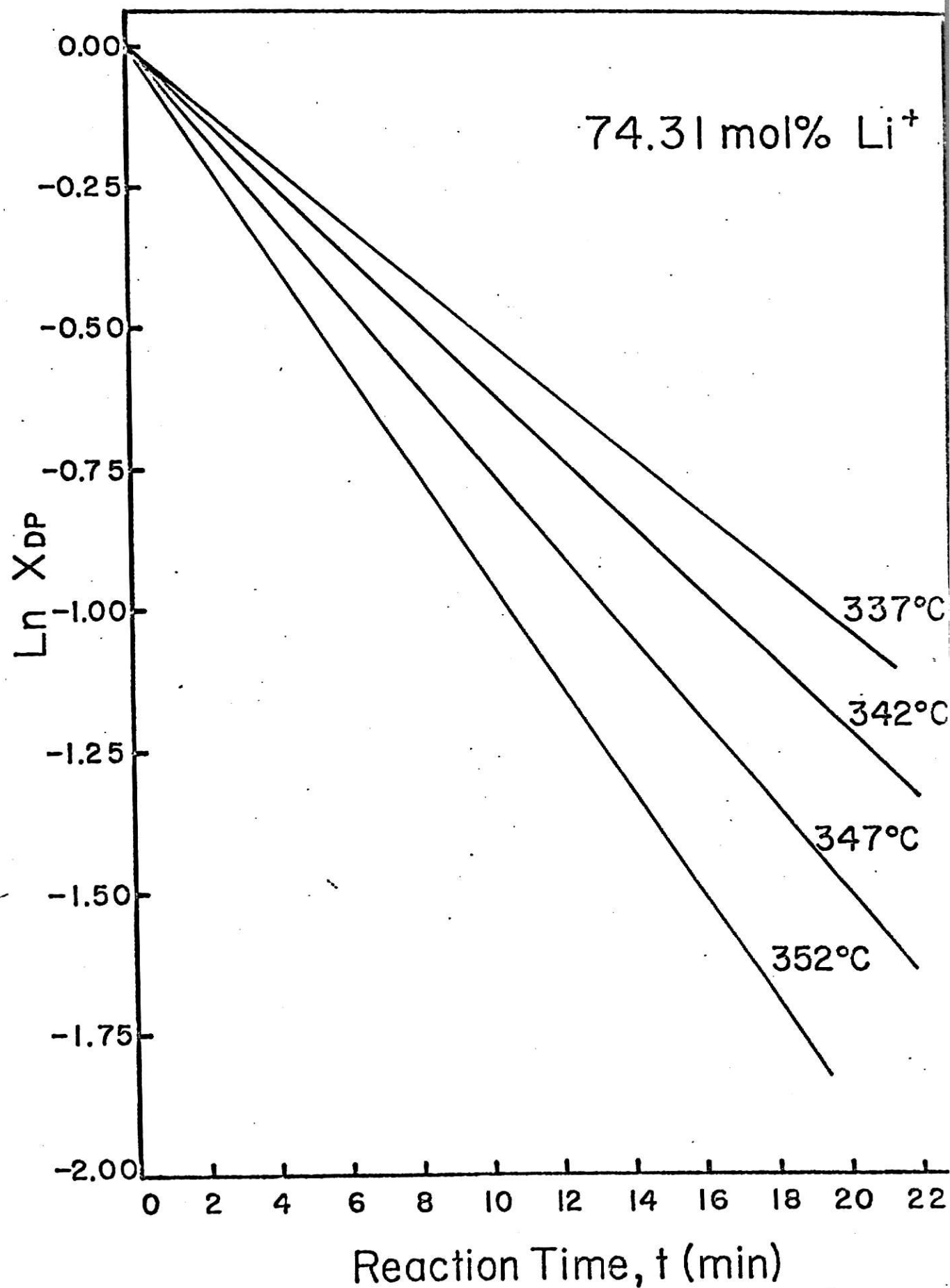
Fig. 15. Plots of the natural logarithm of the fraction of unreacted diphosphate anion, $\ln X_{DP}$, versus reaction time, t (min), at various temperatures for the reaction of $P_2O_7^{4-}$ in molten $LiNO_3$ solvent of 65.30 cation mol % Li^+ .



Explanation of Plate XI.

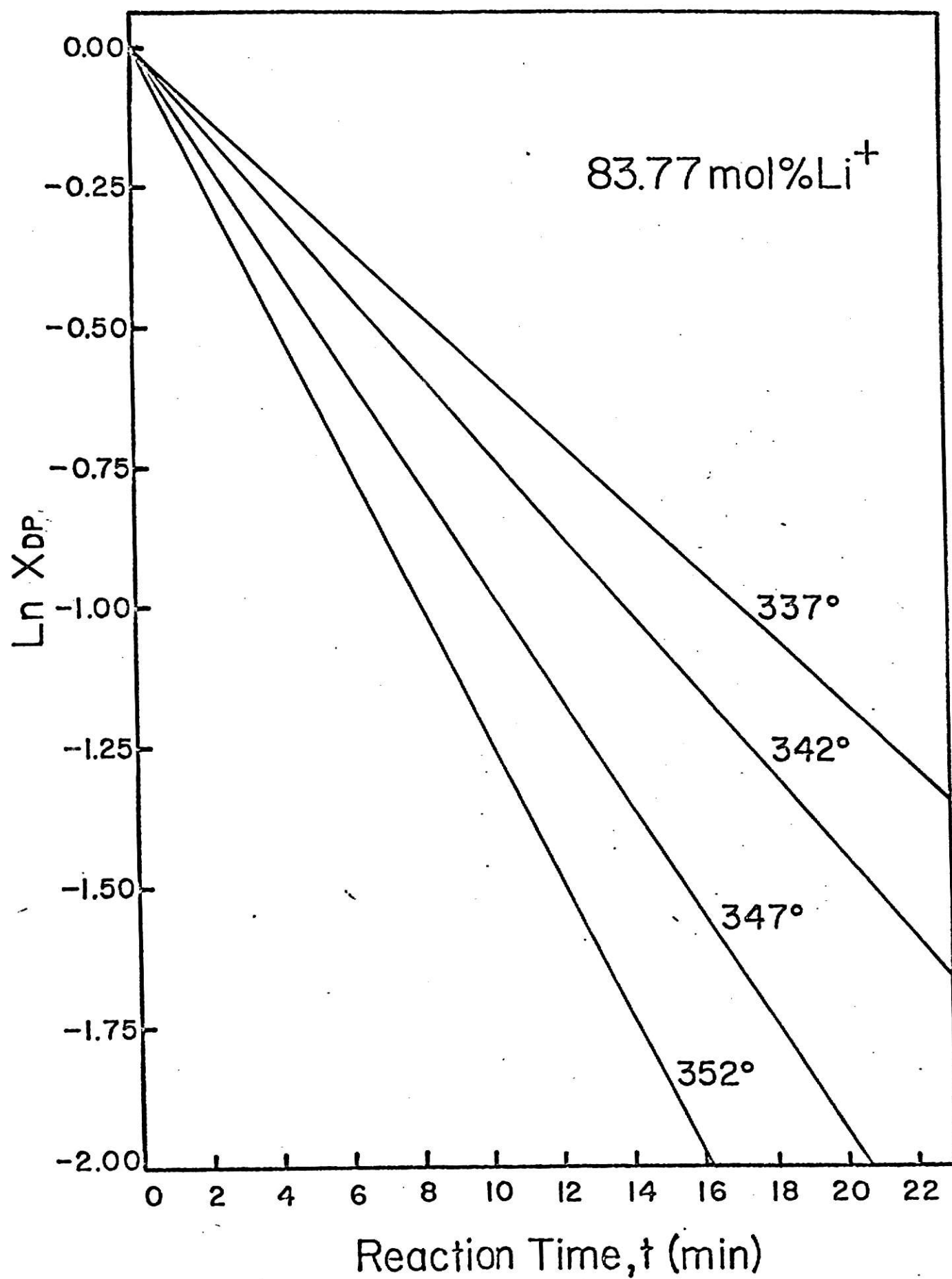
Fig. 16. Plots of the natural logarithm of the fraction of unreacted diphosphate anion, $\ln X_{DP}$, versus reaction time, t (min), at various temperatures for the reaction of $P_2O_7^{4-}$ in molten $LiNO_3$ solvent of 74.31 cation mol % Li^+ .

Plate XI



Explanation of Plate XII.

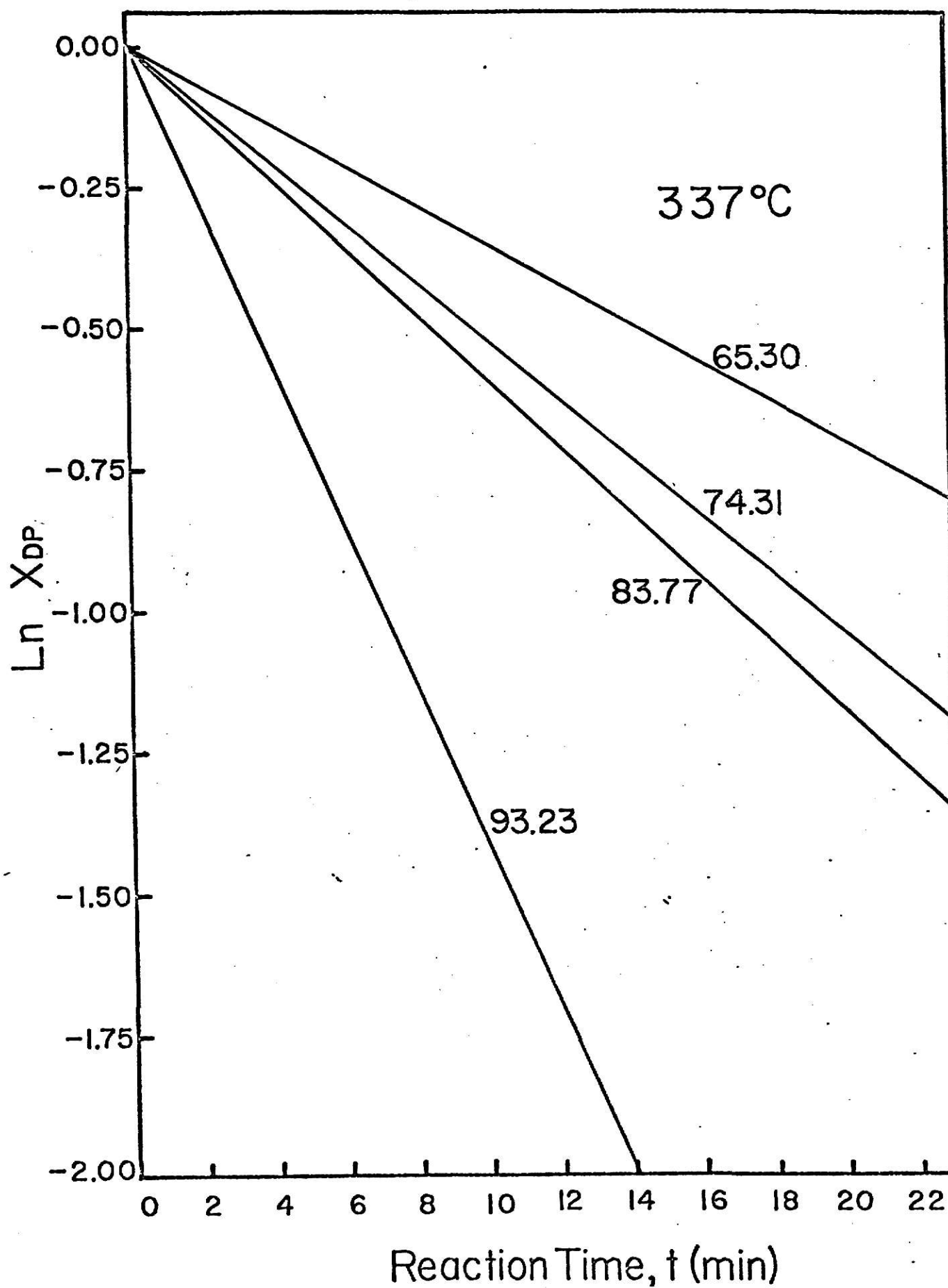
Fig. 17. Plots of the natural logarithm of the fraction of unreacted diphosphate anion, $\ln X_{DP}$, versus reaction time, t (min), at various temperatures for the reaction of $P_2O_7^{4-}$ in molten $LiNO_3$ solvent of 83.77 cation mol % Li^+ .



Explanation of Plate XIII.

Fig. 18. Plots of the natural logarithm of the fraction of unreacted diphosphate anion, $\ln X_{DP}$, versus reaction time, t (min), at various Li^+ concentrations for the reaction of $\text{P}_2\text{O}_7^{4-}$ in molten LiNO_3 solvent at 337° .

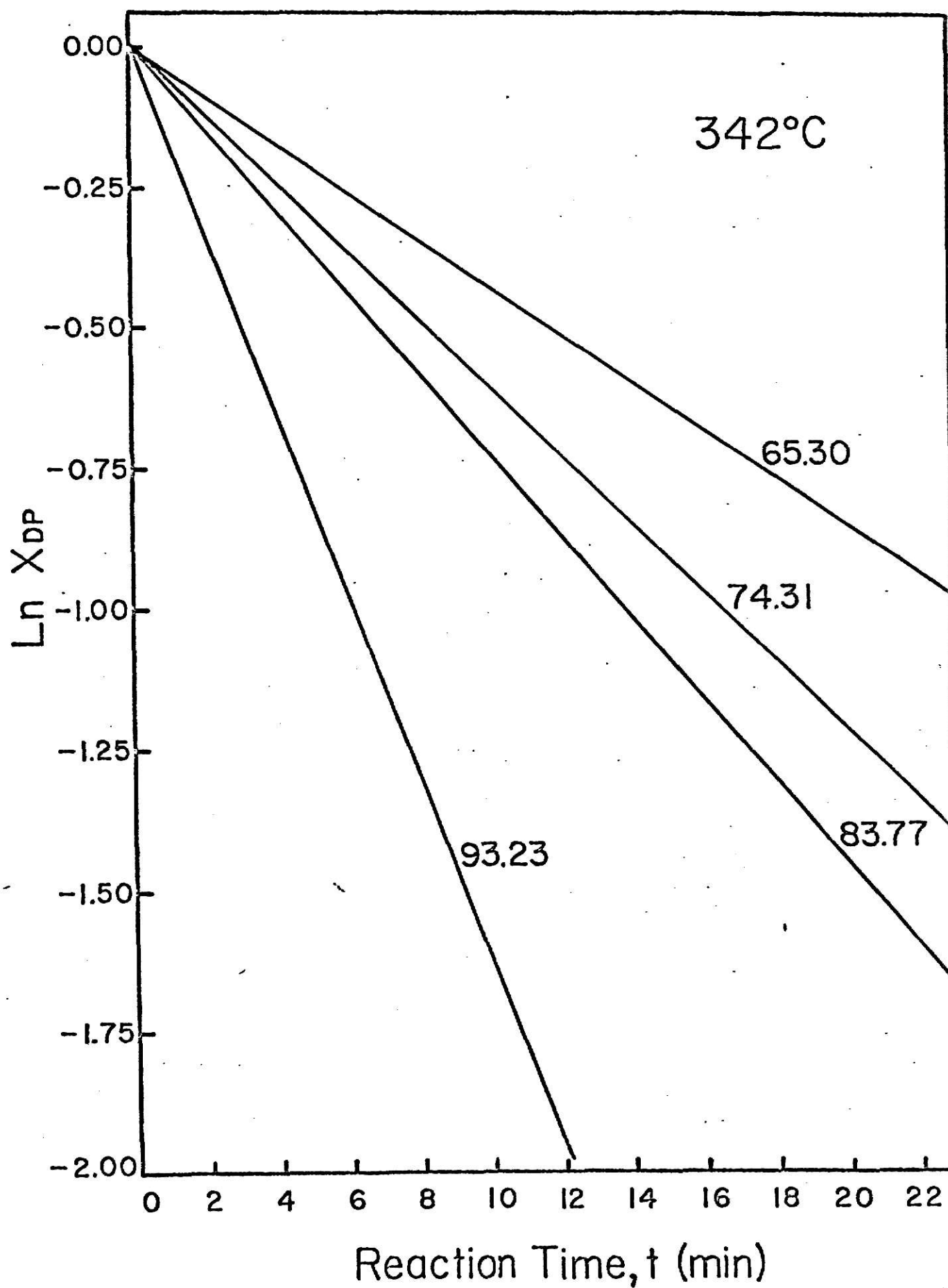
Plate XIII



Explanation of Plate XIV.

Fig. 19. Plots of the natural logarithm of the fraction of unreacted diphosphate anion, $\ln X_{DP}$, versus reaction time, t (min), at various Li^+ concentrations for the reaction of $\text{P}_2\text{O}_7^{4-}$ in molten LiNO_3 solvent at 342° .

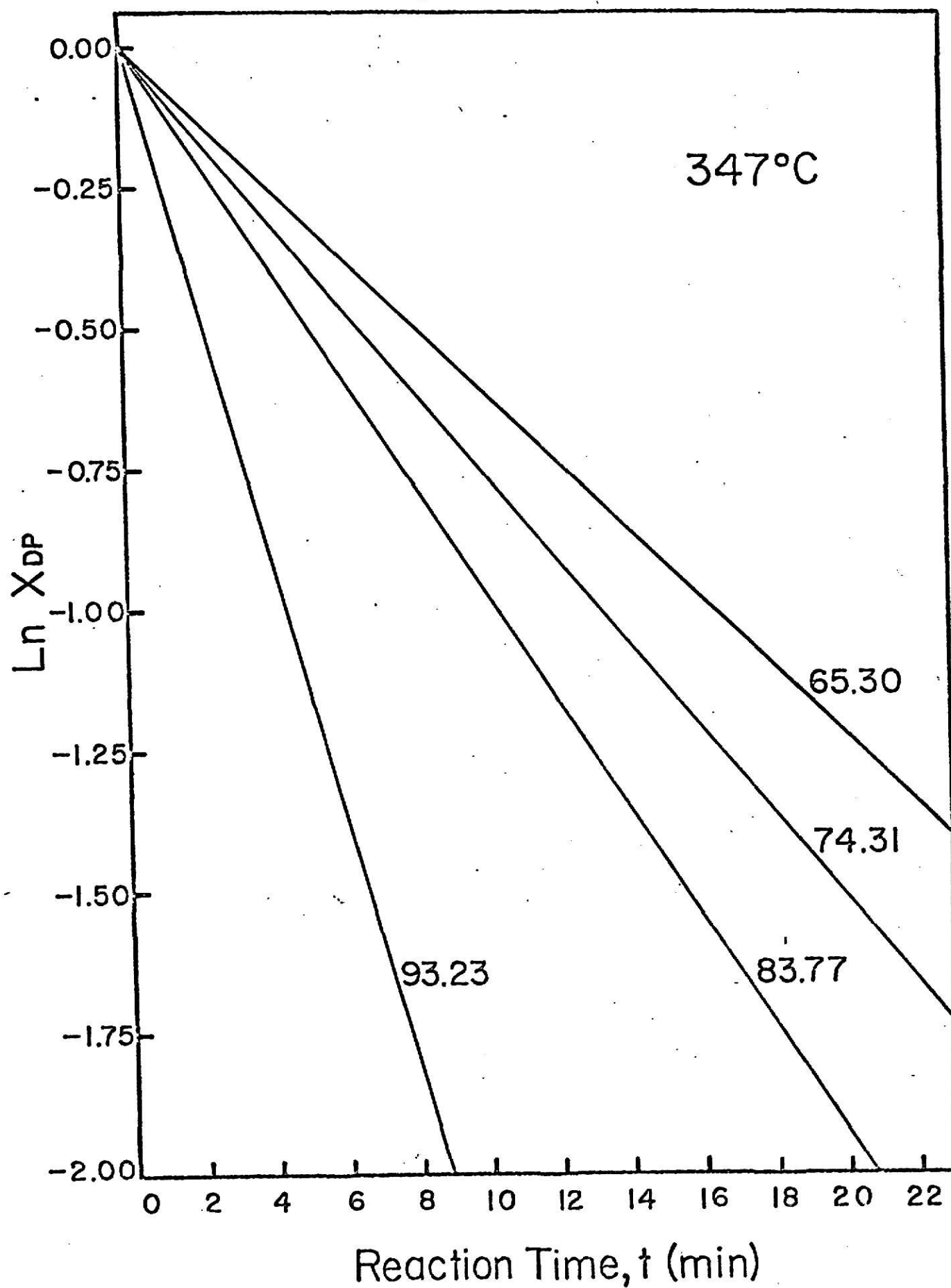
Plate XIV



Explanation of Plate XV.

Fig. 20. Plots of the natural logarithm of the fraction of unreacted + diphosphate anion, $\ln X_{DP}$, versus reaction time, t (min), at various Li^+ concentrations for the reaction of $P_2O_7^{4-}$ in molten $LiNO_3$ solvent at 347° .

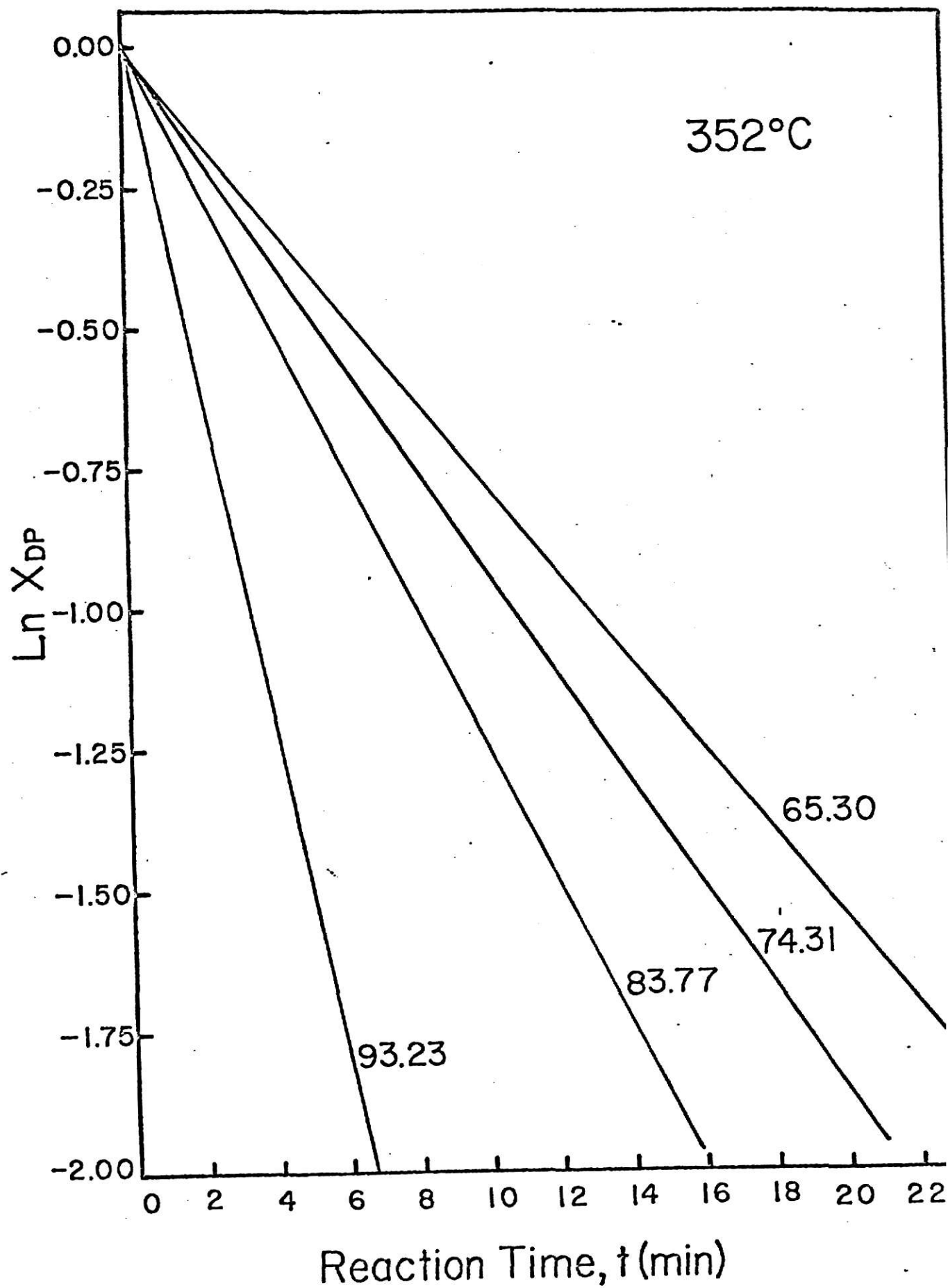
Plate XV



Explanation of Plate XVI.

Fig. 21. Plots of the natural logarithm of the fraction of unreacted + diphosphate anion, $\ln X_{DP}$, versus reaction time, t (min), at various Li^+ concentrations for the reaction of $\text{P}_2\text{O}_7^{4-}$ in molten LiNO_3 solvent at 352° .

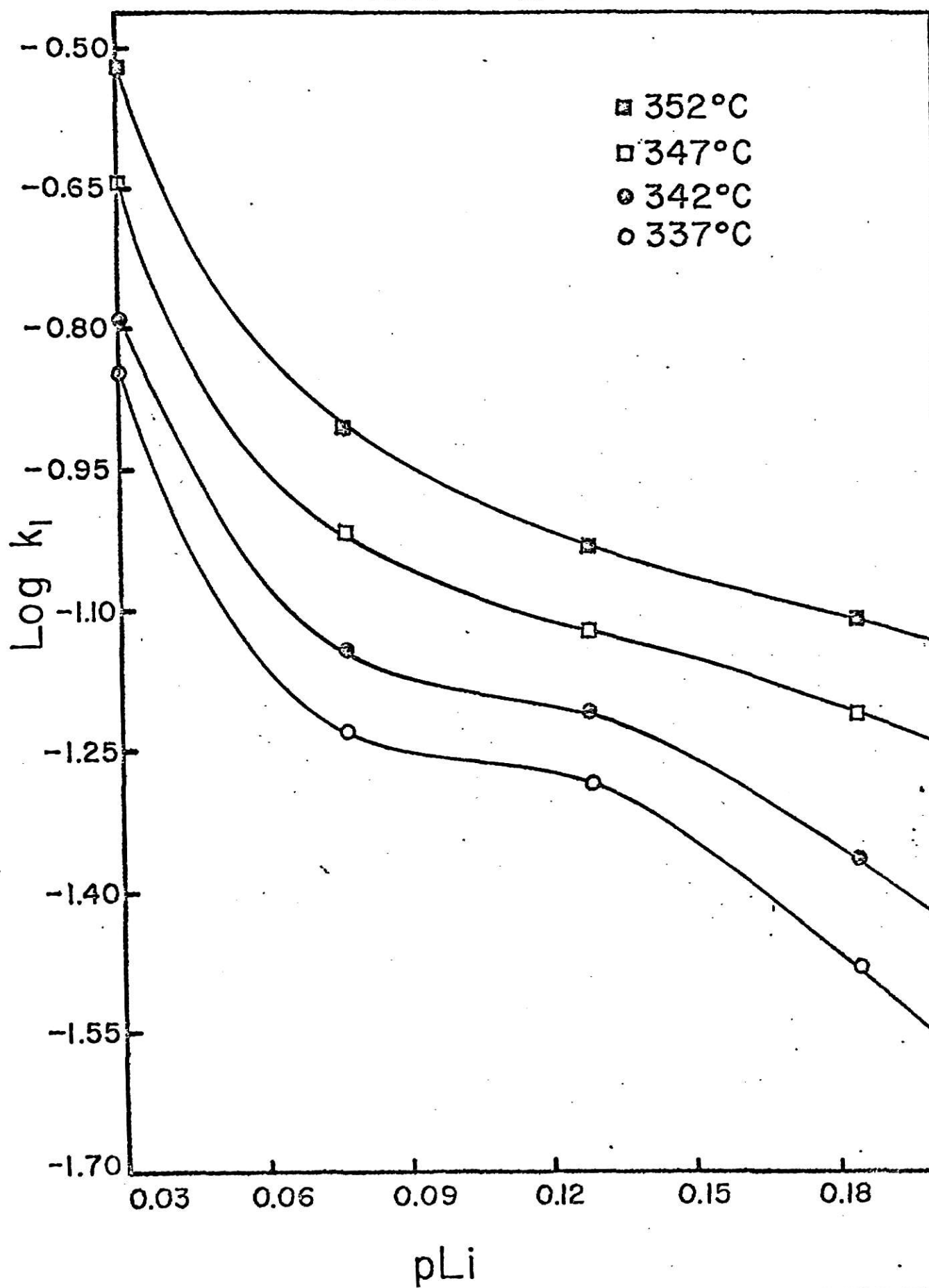
Plate XVI



Explanation of Plate XVII.

Fig. 22. Plots of the common logarithm of the first order rate constants, $\log k_1 \text{ (min)}^{-1}$, versus the negative common logarithm of the Li^+ cation concentration, pLi , at various temperatures.

Plate XVII



cation mol % Li^+ work of Hubble. The temperature was 337° for all the runs of Figure 18. Figures 19 through 21 illustrate the comparisons of the different concentrations of Li^+ at 342° , 347° , and 352° , respectively.

Figure 22 is a comparison of the rate constants with the concentration of Li^+ . This comparison is shown by a plot of the common logarithm of the first order rate constants, $\log k_1$, versus the negative common logarithm of the cation mol % Li^+ , ($-\log \text{Li}^+$, defined as pLi). This is the same type of plot used to compare hydrolysis rate constants as a function of pH (6). The curves obtained have a similar trend to those of the hydrolysis work.

SUMMARY AND CONCLUSIONS

The purpose of this research was to obtain kinetic data for the reaction of $\text{Na}_4\text{P}_2\text{O}_7$ in molten LiNO_3 , and to compare these data as functions of Li^+ concentration and temperature. As it was shown by Gutierrez (5) and Hubble that a Li^+ cation effect existed in the degradation of condensed phosphates in molten alkali nitrates, it seemed worthwhile to examine the concentration effects of the Li^+ catalyst on the above reaction. Also, as work on the hydrolysis of condensed phosphates as a function of H^+ concentration have been examined (6), comparisons of the degradation results in molten alkali nitrates to those of hydrolysis seemed plausible.

As explained previously the lower practical limits of kinetic study seemed to be at a Li^+ concentration of 65.30 cation mol % and at a temperature of 337° . The reason for this lower limit in Li^+ concentration is unknown, but is presumed to be the result of the formation of a precipitate at lower concentrations, thereby causing inability to obtain effective kinetic data.

As summarized in Table 9 the activation energies obtained are in the range from 30 to 50 kcal mol^{-1} . These compare favorably with activation energies of hydrolysis studies which vary from 30 to 40 kcal mol^{-1} , as conducted in solutions of pH 4 to 10 (6). The activation entropies did not correlate as well. The results of the present work range from -5 to -30 e.u. mol^{-1} , while hydrolysis values range from -5 to -1 e.u. mol^{-1} (6). The hydrolysis values were again for reactions occurring in solutions of pH 4 to 10. The lack of resemblance of the activation entropies can best be explained in terms of extrapolation errors resulting from the short temperature range studied in the molten nitrate work.

The foregoing facts support the mechanism proposed by Hubble and Cope-land to interpret the degradation of the diphosphate anion, $\text{P}_2\text{O}_7^{4-}$, in molten alkali nitrates. The proposed $\text{S}_{\text{N}}1$ mechanism, shown in reactions 19a through 19c, is similar to that proposed for the hydrolysis reaction. The main differences are the replacement of Li^+ by H^+ , and instead of the donation of $[\text{O}^{2-}]$ (from excess NO_3^-) to PO_3^- , illustrated in reaction 19b, there is a nucleophilic attack by H_2O on this monometaphosphate anion, and the elimination of reaction 19c.

Figure 22 shows a plot of $\log k_1$ versus $-\log \text{Li}^+$ concentration as cation mole percent (defined as pLi). This plot seems to have some of the characteristics of the hydrolysis plots of Figure 4. The similarity of the curves is good, however the comparison is not reliable because of inability to align the concentration scales of both plots. The comparisons are sufficient, however to make use of ideas employed in interpreting the change in hydrolysis rate as a function of H^+ concentration. Thus, a possible interpretation of what might have been occurring in the present study is that a change in the form of a lithium complexed diphosphate anion, $\text{Li}_n\text{P}_2\text{O}_7^{(4-n)-}$, present in the reacting system, resulted in a rate constant change. This would be analogous to the change in degree of protonation of $\text{P}_2\text{O}_7^{4-}$ with pH altering the hydrolysis rate constant. However, not enough information has been accumulated to conclude positively that the mechanism is correct, or that the change in rate observed as a function of Li^+ concentration can be interpreted in the manner discussed.

Future studies should examine larger chain and cyclic condensed phosphate reactions with various concentrations of molten LiNO_3 and include comparisons with hydrolytic work that have been completed. Also, the possible determination of the structures of the lithium complexed diphosphate anions and also the determination of their concentration in molten nitrate solvents of given lithium concentrations should be made. A study of lithium salts of the condensed phosphates in molten sodium nitrate may be of some benefit to comparisons with hydrolytic work. The possible examination of these lithium salts may yield a cross check on work done in molten lithium nitrate.

ACKNOWLEDGMENTS

The author wishes to acknowledge the encouragement, patience, and support given to him by Dr. J. L. Copeland during the course of this and the related work necessary to the completion of this Master's Degree.

A very deep appreciation is extended to Bonnie, Kimberly, and Sean, the author's wife, daughter, and son. Their patience and faith, as well as the sacrifices made by them during the attainment of this goal will always be remembered.

The author also gratefully acknowledges support of this work by the National Science Foundation, Grant No. GP-12002.

LITERATURE CITED

1. D. H. Kerridge, "Inorganic Chemistry Series 1," Vol 2, C. C. Addison and D. B. Sewerby, Ed., MTP International Review of Science, 1972, pp 29-60.
2. K. W. Fung and G. Mamantov, "Advances in Molten Salt Chemistry," J. Braunstein, G. Mamantov, and G. P. Smith, Ed., Plenum Press, New York, N. Y., London (1973) pp 199-254.
3. H. Lux, Z. Electrochem., 45, 303 (1939).
4. (a) H. Flood and T. Forland, Acta Chem. Scand., 1, 592, 781 (1947); (b) H. Flood, T. Forland, and B. Roald, ibid., 1, 790 (1947); (c) H. Flood, T. Forland, and K. Matzfeldt, ibid., 6, 257 (1952).
5. L. Gutierrez, Ph.D. Thesis, Kansas State University, 1972.
6. R. K. Osterheld in "Topics in Phosphorus Chemistry," Vol. 7, E. J. Griffith and M. Grayson, Ed., Interscience, New York, N. Y., 1972, pp 123-133.
7. L. Gutierrez and J. L. Copeland, J. Phys. Chem., 77, 20 (1973).
8. F. R. Duke and R. N. Kust, J. Amer. Chem. Soc., 85, 3338 (1963).
9. L. E. Topol, R. A. Osteryoung, and J. H. Christie, J. Phys. Chem., 70, 2857 (1966).
10. (a) P. G. Zambonin and J. Jordan, J. Amer. Chem. Soc., 89, 6365 (1967); (b) ibid., 91, 2225 (1969); (c) P. G. Zambonin, Anal. Chem., 41, 868 (1969); (d) P. G. Zambonin, J. Electroanal. Chem., 24, 25A (1970); (e) ibid., 24, 365 (1970).
11. F. R. Duke and S. Yamamoto, J. Amer. Chem. Soc., 81, 6378 (1959).
12. J. R. Moyer, Dow Chemical Co., private communication to L. E. Topol, R. A. Osteryoung, and J. H. Christie, Referenced in J. Phys. Chem., 70, 2857 (1966).
13. B. J. Brough, D. A. Habboush, and D. H. Kerridge, J. Inorg. Nucl. Chem., 30, 2870 (1968).
14. R. N. Kust, Inorg. Chem., 3, 1035 (1964).
15. P. G. Zambonin, J. Electroanal. Chem., 24, 365 (1970).
16. P. G. Zambonin, Anal. Chem., 44, 763 (1972).
17. P. G. Zambonin, ibid., 43, 1571 (1971).

18. M. Francini and S. Martini, Electrochim. Acta, 13, 851 (1968).
19. A. M. Shams El Din, ibid., 7, 285 (1962).
20. A. M. Shams El Din and A. A. A. Gerges, Proc. First Aust. Conf. Electrochem., Pergamon Press, Oxford, 1963, p 462.
21. P. G. Zambonin, J. Electroanal. Chem., 33, 243 (1971).
22. R. B. Temple, M. Fredericks, and G. W. Thickett, J. Electroanal. Chem., 38, A5 (1972).
23. R. N. Kust, J. Electrochem. Soc., 116, 1137 (1969).
24. A. M. Shams El Din and A. A. El Hosary, J. Inorg. Nucl. Chem., 28, 3043 (1963).
25. J. R. Van Wazer, "Phosphorus and its Compounds," Vol. 1, Interscience, New York, N. Y., 1958, pp 419-478, 601-716.
26. H. J. Emeleus and A. G. Sharpe, "Modern Aspects of Inorganic Chemistry," John Wiley and Sons, New York, N. Y., 1973, pp 304-315.
27. (a) A. M. Shams El Din, A. A. El Hosary, and A. A. A. Gerges, J. Electroanal. Chem., 6, 131 (1963); (b) ibid., 8, 312 (1964); (c) A. M. Shams El Din and A. A. A. Gerges, Electrochim. Acta, 9, 123 (1964); (d) A. M. Shams El Din and A. A. El Hosary, ibid., 13, 135 (1968); (e) A. A. El Hosary and A. M. Shams El Din, ibid., 16, 143 (1971); (f) A. M. Shams El Din, H. D. Taki El Din, and A. A. El Hosary, ibid., 13, 407 (1968).
28. W. J. Youden, "Statistical Methods for Chemists," John Wiley and Sons, New York, N. Y., 1951, pp 45-49.
29. S. W. Benson, "The Foundations of Chemical Kinetics," McGraw Hill, New York, N. Y., 1960, pp 66-73 .
30. J. H. R. Clarke and G. J. Hills, Chem. Brit., 9, 12 (1973).
31. Ref. 6 pp 114-123.
32. J. J. Lagowski, "Modern Inorganic Chemistry," Marcel Dekker, New York, N. Y., 1973, pp 659-660.
33. Ibid., pp 228.
34. Ref. 25 pp 457-458.
35. M. M. Crutchfield and R. R. Irani, J. Amer. Chem. Soc., 7, 2815 (1965).
36. B. R. Hubble and J. L. Copeland, J. Chem. Eng. Data, 15, 441 (1970).
37. Kindly constructed by M. Ohno, Physics Dept., Kansas State University, Manhattan, Kansas.

VITA

The author was born in Pittsburg, Kansas, on January 18, 1950, to Richard and Betty Metcalf. He attended public grade schools in Pittsburg and Emporia, Kansas, and graduated from Emporia Senior High School in 1968. He received the Bachelor of Arts degree from Kansas State Teachers College in 1972; and the Master of Science degree from Kansas State University in 1975.

He and the former Bonita Jean Nickell, of Parker, Kansas, were married on August 14, 1971. A daughter, Kimberly Ann, was born to them on March 13, 1972; and a son, Sean Richard, was born to them on November 17, 1974.

He is a member of the Beta Rho chapter of Alpha Chi Sigma Fraternity of Professional Chemists.

THE EFFECT OF LITHIUM ION ON THE DEGRADATION
OF DIPHOSPHATE ANION IN MOLTEN ALKALI NITRATES

by

ARTHUR STEVEN METCALF

B.A. Kansas State Teachers College, 1972

AN ABSTRACT OF A MASTER'S THESIS

submitted in partial fulfillment of the

requirements for the degree

MASTER OF SCIENCE

Department of Chemistry

KANSAS STATE UNIVERSITY

Manhattan, Kansas

1975

Effects of Li^+ cation concentrations on the reaction kinetics of $\text{P}_2\text{O}_7^{4-}$ with NO_3^- (as molten alkali nitrates) were investigated. Concentrations of Li^+ were 65.30, 74.31, and 85.77 cation mol %, with Na^+ as the remaining cation. The reactions were studied at 337, 342, 347, and 352°C at each of the above Li^+ concentrations.

The reactions were followed by ^{31}P nmr analyses of aqueous solutions of quenched samples at various times, for given Li^+ concentrations and temperatures. The ^{31}P nmr spectra contained only signals from phosphorus atoms of the reactant, $\text{P}_2\text{O}_7^{4-}$, and the product, PO_4^{3-} . From integrated intensities of the signals, relative concentrations of reactant and product were found. As the reaction is first order in $\text{P}_2\text{O}_7^{4-}$, plots of the natural logarithm of the fraction of unreacted diphosphate anion, $\ln X_{\text{DP}}$, versus time, t (min), were made. These plots yielded first order rate constants from least squares analyses of the slopes of best straight lines forced through the origin. Least squares equations for straight lines of Arrhenius plots for each of the three Li^+ concentrations were:

$$\begin{aligned} 65.30 \text{ Li}^+ \text{ cation mol \%: } \ln k_1 &= (32.92 \pm 1.54) - (2.22 \quad 0.10) \times 10^4 (1/T) \\ 74.31 \text{ Li}^+ \text{ cation mol \%: } \ln k_1 &= (21.68 \pm 1.15) - (1.50 \quad 0.09) \times 10^4 (1/T) \\ 85.77 \text{ Li}^+ \text{ cation mol \%: } \ln k_1 &= (28.77 \pm 1.28) - (1.93 \quad 0.10) \times 10^4 (1/T) \end{aligned}$$

Activation energies were: (44.04 ± 1.89) , (29.89 ± 1.41) , and (38.33 ± 1.57) kcal mol $^{-1}$ for the 65.30, 74.31, and 85.77 cation mol % Li^+ concentrations, respectively. A comparison of rate constants as a function of the concentration of Li^+ showed similarities to investigations of hydrolysis of the diphosphate anion, $\text{P}_2\text{O}_7^{4-}$, as a function of H^+ concentration. In these latter studies it is believed that the change in rate is affected by a change in the type of protonated species present in solution at a given pH. Thus it can be postulated that the change in rate observed in the present studies is due to a change in the number of Li^+ cations complexed with terminal oxygens of the diphosphate anion.